A PROPOSAL TO DEFINITIVELY DETERMINE THE CONTRIBUTION OF MULTIPLE PHOTON EXCHANGE IN ELASTIC LEPTON-NUCLEON SCATTERING

THE OLYMPUS COLLABORATION

September 9, 2008

THE OLYMPUS COLLABORATION

Arizona State University, USA
DESY,Hamburg, Germany
Hampton University, USA
INFN, Bari, Italy
INFN, Ferrara, Italy
INFN, Rome, Italy
Massachusetts Institute of Technology, USA
St. Petersburg Nuclear Physics Institute, Russia
Universität Bonn, Germany
University of Colorado, USA
Universität Erlangen-Nürnberg, Germany
University of Glasgow, United Kingdom
University of Kentucky, USA
Universität Mainz, Germany
University of New Hampshire, USA

Contents

Chapter 1

Overview of the Experiment

1.1 Introduction

Recent determinations of the proton electric to magnetic form factor ratio from polarization transfer measurements at JLab indicate an unexpected and dramatic discrepancy with the form factor ratio obtained using the Rosenbluth separation technique in unpolarized cross section measurements. This discrepancy has been explained as the effects of multiple photon exchange beyond the usual one-photon exchange approximation in the calculation of the elastic electron-proton scattering cross section. Since most of our understanding on the structure of the proton and atomic nuclei is based upon lepton scattering analyzed in terms of the single photon approximation; it is essential to definitively verify the contribution of multiple photon exchange.

In June 2007, our collaboration submitted to DESY a letter of intent to carry out an experiment to definitively determine the contribution of multiple photon exchange in elastic lepton-nucleon scattering. The most direct evidence for multiple photon exchange would be a deviation from unity in the ratio of positron-proton to electron-proton elastic scattering cross sections. The experiment would utilize intense beams of electrons and positrons in the DORIS ring incident on an internal hydrogen gas target at an incident energy of 2.0 GeV and precisely measure elastic scattering at polar angles between 20° and 80° with high statistical and systematic precision. For this experiment we proposed to use the existing Bates Large Acceptance Spectrometer Toroid (BLAST) from MIT and an unpolarized internal gas target similar to one used by the HERMES experiment at HERA.

The letter of intent was favorably reviewed by the DESY Physics Research Committee at its Fall 2007 meeting. By May 2008, the experiment had been studied by the DESY machine group and it was determined that the experiment was feasible. Further, the proposed experiment can be installed and commissioned in parallel with existing light source operation at DORIS but will require dedicated data taking time. A formal proposal was invited.

The OLYMPUS (p**O**sitron-proton and e**L**ectron-proton elastic scattering to test the h**Y**pothesis of **M**ulti-**P**hoton exchange **U**sing dori**S**) collaboration comprises over fifty physicists from fifteen institutions in Germany, Italy, Russia, the United Kingdom, and the United States. This document describes in detail the proposed OLYMPUS experiment. OLYMPUS is made possible by the availability of a great deal of existing equipment (>$ 5 million in-

vestment) from the recently completed BLAST experiment at MIT-Bates. The design of OLYMPUS has been carefully optimized to keep the operating costs low. Three months of dedicated beam time at 2 GeV on the DORIS ring are requested to carry out the OLYMPUS experiment.

The proposal is divided into three chapters. Chapter 1 is an overview of the experiment. It presents the physics motivation, describes the principle of the experiment, and the anticipated precision for the measured ratio of cross-sections. Chapter 2 describes the impact on the DORIS ring and contains a discussion of the technical aspects of the experiment including a detailed description of the BLAST spectrometer, detectors, internal target, luminosity monitor, and the expected backgrounds. Chapter 3 addresses the logistics of the experiment and describes the necessary budget, the manpower in the OLYMPUS collaboration, and the requests to DESY.

In summary, the current, dramatic discrepancy between recoil polarization and Rosenbluth measurements of the proton elastic form factor ratio constitutes a serious challenge to our understanding of the structure of the proton. The widely accepted explanation in terms of multiple photon exchange demands a definitive confirmation. A precision measurement of the e^+p/e^-p elastic cross section ratio will directly test the contribution of multiple photon effects. As the prediction of the magnitude of multiple photon effect is model-dependent, the experiment described here will provide a strong constraint to theoretical calculations. The experiment takes advantage of unique features of the BLAST detector combined with an internal hydrogen gas target and the DORIS storage ring operated with both electrons and positrons. The systematic uncertainties are controllable at the percent level, and with the superior luminosity that can be provided at DORIS, this experiment will not be limited in statistical precision.

1.2   Physics Motivation

In the course of the more than 50 year long history of elastic electron-proton scattering since Hofstadter [1] the separation of the proton's electric and magnetic form factors, $G_E^p(Q^2)$ and $G_M^p(Q^2)$, has been of particular interest. These two functions of Q^2 describe the distribution of charge and magnetism of the proton and it is expected that precise *ab initio* calculations in terms of quarks and gluons will become available in the foreseeable future using lattice QCD techniques [2]. Until the 1990's the experimental method to separate $G_E(Q^2)$ and $G_M(Q^2)$ was based on the procedure by Rosenbluth [3] measuring the unpolarized elastic cross section at fixed four-momentum transfer, Q^2, but with different electron scattering angles and incident beam energies. It was found that the Q^2 dependence of both G_E and G_M, to a good approximation, followed the form of the Fourier transform of an exponentially decaying distribution, namely the dipole form factor $(1 + Q^2/0.71)^{-2}$, implying a ratio of $\mu G_E/G_M \approx 1$ as shown by the open symbols in Figure 1.1 (left panel).

Due to the nature of the Rosenbluth formula

$$\frac{d\sigma/d\Omega}{(d\sigma/d\Omega)_{Mott}} = \frac{G_E^2(Q^2) + \tau G_M^2(Q^2)}{1 + \tau} + 2\tau G_M^2(Q^2)\tan^2\frac{\theta}{2} = \frac{\epsilon\, G_E^2(Q^2) + \tau G_M^2(Q^2)}{\epsilon\,(1 + \tau)}, \quad (1.1)$$

where $\tau = Q^2/(4M_p^2)$, the transverse virtual photon polarization $\epsilon = [1+2(1+\tau)\tan^2(\theta/2)]^{-1}$,
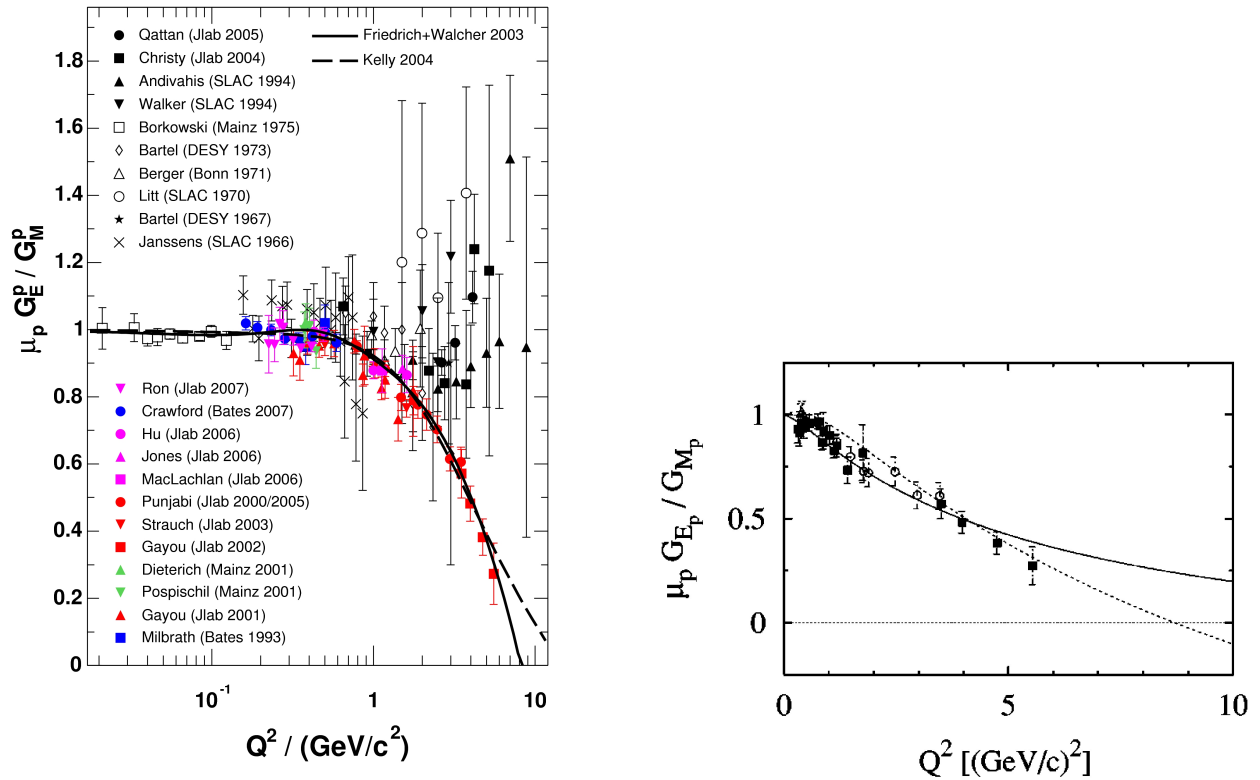
Figure 1.1: Left panel: Proton electric to magnetic form factor ratio from unpolarized measurements (black symbols) using the Rosenbluth method [4, 5, 6] and from double polarization experiments (colored symbols) [7, 8, 9, 10, 11, 12, 13, 14]. Also shown are two recent parameterizations [15, 16]. Right panel: form factor ratio $\mu G_E/G_M$ from recoil polarization compared with calculations by Iachello from 2004 (solid) [17] and 1973 (dashed) [18].

and $(d\sigma/d\Omega)_{Mott} = \alpha^2/(4E^2)\,(\cos^2\frac{\theta}{2}/\sin^4\frac{\theta}{2})(E'/E)$; the weight of G_E in the cross section becomes less at higher Q^2 making the Rosenbluth separation of $G_E(Q^2)$ and $G_M(Q^2)$ at high momentum transfer rather difficult. While some experiments reported a scaling of the form factors, others occasionally observed significant deviations of the ratio $\mu G_E/G_M$ from unity. The world data for elastic e-p scattering have recently been compiled by [19]. The most recent Rosenbluth-type measurements have again confirmed the scaling behavior of the proton form factor ratio [5, 6], and additional unpolarized precision measurements are underway [21].

In the late 1990's, development of polarized beams, targets and polarimeters permitted a new way to measure the form factor ratio more directly through the interference of G_E and G_M in the spin-dependent elastic cross section asymmetry [9, 10, 11, 12]. It came as a big surprise when the high precision polarization transfer measurements at Jefferson Laboratory at higher momentum transfers (up to 5.5 $(GeV/c)^2$) gave striking evidence that the proton form factor ratio $\mu G_E/G_M$ was monotonically falling with Q^2 [7]. This Q^2 dependence was

dramatically different from that observed with the unpolarized Rosenbluth method. Linear extrapolation of the polarization data would even suggest a node of the electric form factor near 8 $(\text{GeV/c})^2$. Note that this decline of the proton form factor ratio was predicted already in 1973 by calculations based on vector-meson dominance including the expected node around 8 $(\text{GeV/c})^2$ [17, 18] shown in Figure 1.1 (right panel). Future recoil polarization experiments at Jefferson Lab will extend the Q^2 range up to 9 $(\text{GeV/c})^2$ with a new recoil polarimeter [22] and up to 14 $(\text{GeV/c})^2$ after the 12 GeV upgrade [23].

Alternative measurements of G_E/G_M are based on the spin-dependent asymmetries with polarized beam and target. Experiments of this kind are considered equivalent to polarization transfer and constitute important independent tests to verify the recoil polarization results. Such measurements have recently been performed with the Bates Large Acceptance Spectrometer Toroid (BLAST) at low Q^2 using an internal polarized hydrogen target [14]. The result is consistent with scaling of the form factor ratio, albeit at low Q^2 where no discrepancy between polarized and unpolarized measurements was expected. Another experiment used a frozen-spin ammonia target [13] to extract the form factor ratio at somewhat higher $Q^2 \approx 1.51$ $(\text{GeV/c})^2$ with a result for $\mu G_E/G_M$ between the unpolarized and polarization transfer data (magenta triangle in left plot of Figure 1.1). Clearly, further measurements are needed to resolve this discrepancy.

The generally accepted explanation for the discrepancy between the recoil polarization and Rosenbluth determinations of the elastic proton form factor ratio is the exchange of multiple (>1) photons during the electron-proton elastic scattering process [24, 25, 26, 27]. This implies that certain lepton-nucleon scattering observables will differ significantly from their one-photon exchange (or first-order Born approximation) expectation value.

Multiple-photon exchange processes will exhibit a characteristic dependence of the elastic lepton-proton scattering cross section on the value of the virtual photon polarization, ϵ. As ϵ decreases, the effects of multiple-photon exchange on the elastic cross section tend to increase in magnitude.

The discrepancy between the recoil polarization and Rosenbluth determinations of the elastic proton form factor ratio grows with increasing Q^2. At high Q^2, the cross section is dominated by magnetic (i.e. transverse) scattering. This explains why the effect on the extraction of G_E from Rosenbluth separations can be sizable, while the effect on the cross section at all values of Q^2 is rather modest. At the same time, the form factor ratio from polarization experiments is less affected.

The effect of multiple-photon exchange on the electromagnetic elastic form factors involves the real part of the multiple-photon exchange amplitude. The observable most sensitive to this amplitude is the ratio of the elastic cross section for electron-proton to positron-proton scattering. In the presence of multiple-photon exchange, the cross section for unpolarized lepton-proton scattering contains an interference term between the one- and two-photon amplitudes. This interference is odd under time reversal, and hence has the opposite sign for elastic positron-proton and electron-proton scattering. Therefore, a non-zero two-photon amplitude would result in different cross sections for unpolarized electron-proton and positron-proton scattering.

Figure 1.2 shows the ratio of the two cross sections as a function of the virtual photon polarization, ϵ, according to [25]. The ratio would be unity in the case of pure single photon exchange, i.e. the Born approximation. The sensitivity is enhanced at low ϵ, exceeding 4%
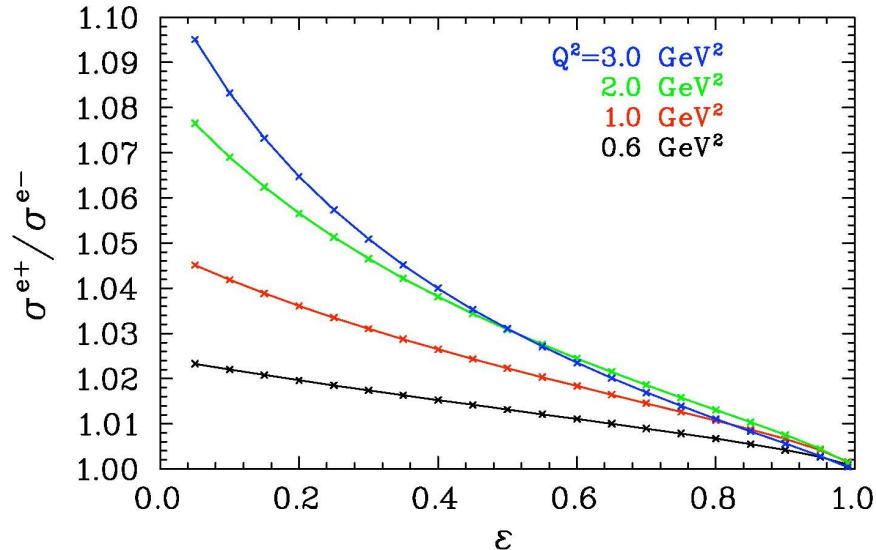
Figure 1.2: Ratio of elastic positron-proton to electron-proton cross section versus virtual photon polarization for given Q^2 [25].

for $\epsilon \leq 0.4$, provided $Q^2 \geq 2$ $(\text{GeV/c})^2$. Beyond $Q^2 = 2$ $(\text{GeV/c})^2$ the Q^2 dependence of the two-photon effect is small, and since the cross section decreases rapidly with Q^2, one would want to keep Q^2 as low as possible for optimized statistics. This is clear in Figure 1.3 which displays the e^+p/e^-p cross section ratio as a function of the scattering angle for three beam energies. Up to scattering angles of about 80°, the cross section ratio is almost independent of the beam energy, and hence of Q^2 for a given scattering angle.

The effects of radiative corrections on the e^+p/e^-p cross section ratio are expected to be negligible. Bethe-Heitler corrections will be identical for positrons and electrons and interference effects which change sign for e^+ and e^-, *e.g.* between the lepton bremsstrahlung process and the proton bremsstrahlung process (a very small effect at these energies) are also expected to be negligible [20].

Figure 1.4 shows the elastic proton electric to magnetic form factor ratio under various conditions: The red diamonds correspond to the form factor ratio as determined from recoil polarization, which has only little sensitivity to multi-photon effects. The magenta crosses correspond to the form factor ratio from existing e^-p Rosenbluth separation data (Bosted fit [28]). The green open circles represent the effect of two-photon exchange on the Rosenbluth measurements, using a simple fit to the two-photon correction that explains the discrepancy between polarization and Rosenbluth measurements. The blue solid circles are the result of applying this two-photon correction to Rosenbluth measurements using e^+p scattering. The expected node at ≈ 2.6 $(\text{GeV/c})^2$ is remarkable. It would correspond to a vanishing slope of the elastic e^+p cross section in the usual Rosenbluth plot as a function of ϵ. Above 2.6 $(\text{GeV/c})^2$, one would expect to find negative values for $G_E^{p\,2}$ from e^+p Rosenbluth separations, corresponding to negative slopes in the Rosenbluth plot.

Previous experiments from the 1960's at SLAC [29] have measured the e^+p/e^-p cross section ratio. However, high-precision measurements with uncertainties of $\approx 1\%$ were done only at low Q^2 or very large ϵ, where the multiple-photon exchange effects appear to be small.
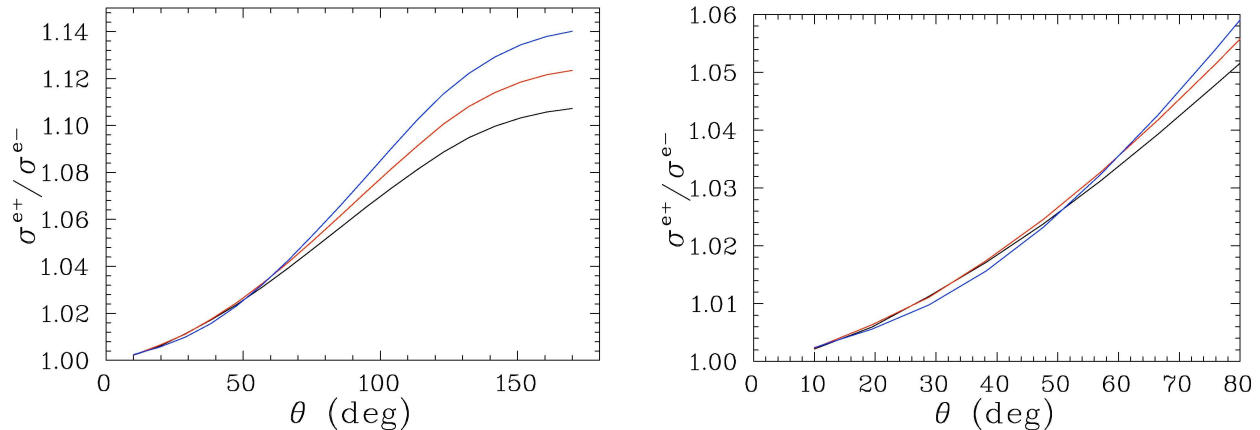
Figure 1.3: e^+p/e^-p cross section ratio as a function of scattering angle, for three beam energies (black=2.0 GeV, red=2.5 GeV, blue=3.0 GeV) [25]. The figure on the right shows the region up to 80° where only little energy dependence of the two-photon effect is evident.

Measurements at low ϵ had uncertainties of $\approx 5\%$, too large to see conclusive deviations from unity. Recent reanalysis of the (limited) low-ϵ data give an indication of multiple-photon exchange effects, consistent with recent calculations, but only at the three-sigma level [19].

Recently, two new experiments have been proposed to study the e^+p and e^-p cross section ratio: one at Jefferson Lab [30] using a secondary electron/positron beam from a pair production target, and another at Novosibirsk [31] based on stored electron and positron beams incident on an internal unpolarized hydrogen target, which will be discussed in Sec. 1.6.

The effect of two-photon exchange on the real part of the lepton-nucleon scattering amplitude can also be investigated by studying the ϵ-dependence of the proton form factor ratio from polarization experiments. Such an experiment has been proposed at Jefferson Lab [32]. Precise mapping of Rosenbluth cross sections in unpolarized e^-p scattering will also reveal any nonlinearities in the ϵ-dependence of the cross section [21].

The imaginary part of the two-photon amplitude would give rise to non-zero transverse single-spin asymmetries, of either the beam (A_n), the target (A_y) or the induced polarization (P_y). These single-spin asymmetries will be studied at Jefferson Lab as well [32, 33].

In this document, we argue that the use of the intense, multi-GeV stored electron and positron beams at the storage ring DORIS at DESY, Hamburg, Germany in combination with the BLAST detector can produce the most definitive data to determine the effect of multiple photon exchange in elastic lepton-proton scattering and verify the recent theoretical predictions.

1.3   Radiative Corrections

The elastic form factors of the proton are defined in the context of the Born cross section, *i.e.* the single photon exchange term in the perturbative QED expansion. Corrections for radiative processes involving the incoming and outgoing charged particles must be applied to
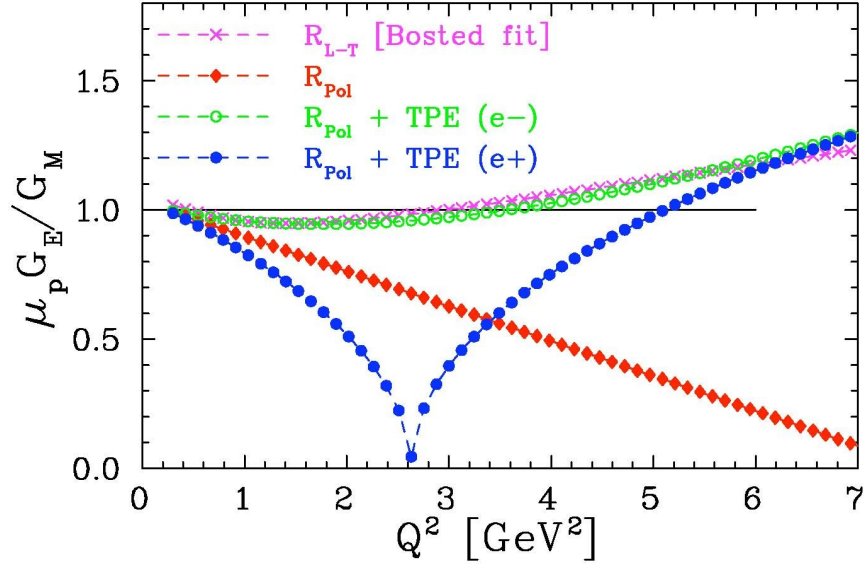
Figure 1.4: Proton electric to magnetic form factor ratio $\mu_p G_E^p / G_M^p$ without (red diamonds) and with two-photon effects calculated for $e^- p$ (green open circles) and $e^+ p$ (blue solid circles) Rosenbluth separations [25]. The magenta crosses represent a fit to existing Rosenbluth-separated $e^- p$ data. The electric form factor G_E^p from unpolarized $e^+ p$ scattering has a node expected at $Q^2 \approx 2.6$ (GeV/c)^2, with $G_E^{p\,2} < 0$ for $Q^2 > 2.6$ (GeV/c)^2.

extract the Born cross section. These corrections are well understood and are calculable in QED. Figure 1.5 shows the leading processes which must be considered for this experiment. The leading Feynman diagram $M_{Born}^{(1)}$ together with vertex corrections, vacuum polarization, and bremsstrahlung are called the Born approximation. The two two-photon exchange diagrams in figure 1.5 are beyond the Born approximation and their measurement is the focus of this proposal.

Most of the terms in Figure 1.5 are identical for electron- and positron-proton elastic scattering, and so determination of the charged lepton ratio is the most sensitive test of the contribution beyond single photon exchange. The amplitude for elastic ep-scattering to order α_{em}^2 can be written as

$$M_{ep \to ep} = e_e e_p M_{Born} + e_e^2 e_p M_{e-brems} + e_e e_p^2 M_{p-brems} + e_e^2 e_p^2 M_{2\gamma}$$

where e_e and e_p are the lepton and proton charges, respectively, and the amplitudes M_{Born}, $M_{e-bremm}$, $M_{p-bremm}$, and $M_{2\gamma}$ describe the amplitudes for one-photon exchange, electron bremsstrahlung, proton bremsstrahlung and two-photon exchange, respectively. Note that radiative processes such as vertex corrections and vacuum polarization do not contribute to the lepton charge asymmetry and are not included here. Squaring the amplitude and keeping corrections to the Born approximation up to order α_{em} that have odd powers of the lepton charge, we have

$$|M_{ep \to ep}|^2 = e_e^2 e_p^2 [|M_{Born}|^2 + 2 e_e e_p M_{Born} Re(M_{2\gamma}^*) + 2 e_e e_p Re(M_{e-bremm} M_{p-bremm}^*)]$$

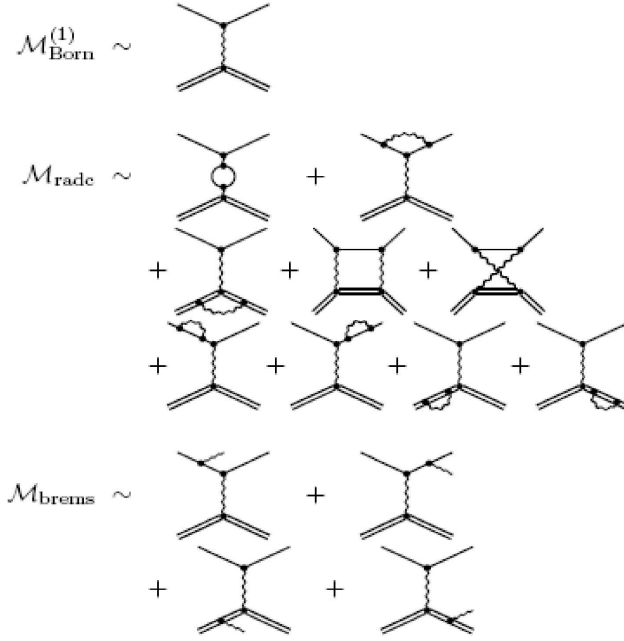where Re denotes the real part of the amplitude.

10

Figure 1.5: The Feynman diagrams beyond leading order for elastic electron/positron-proton elastic scattering [35].

Corrections with an even power of lepton charge do not give rise to any lepton charge asymmetry, *e.g.* the largest correction due to electron bremsstrahlung. The last term above describes interference between electron and proton bremsstrahlung. It is dominated by soft-photon emission and results in a calculable correction which is included in standard approaches to radiative corrections. After correction for this term, one is left with a lepton charge asymmetry which is due only to two-photon exchange.

1.4   Description of the OLYMPUS Experiment

We propose to measure the ratio of electron-proton to positron-proton elastic cross sections over a range of ϵ with the BLAST detector using an internal, unpolarized hydrogen target and intense stored beams of unpolarized positrons and electrons at an energy of 2.0 GeV at the site of the ARGUS experiment on the storage ring DORIS at DESY in Hamburg, Germany. To carry out this experiment it will be required:

- to operate the DORIS storage ring at an energy of 2.0 GeV,

- to switch between beams of electrons and positrons at a frequency on the order of once per day,

- to relocate the BLAST detector from MIT-Bates to DESY/DORIS, and

- to install an unpolarized hydrogen internal gas target in the DORIS storage ring.

11

At DORIS, both electron and positron beams can be stored with high intensity and energies up to 4.5 GeV. The DORIS storage ring was operated as an e^+e^- collider until 1993, and is currently used as a source for synchrotron radiation using ≈ 150 mA positrons with a lifetime of about 20 hours. Comparable beam intensities for electrons as for positrons are anticipated. With modification of the ring magnet power supplies, it is expected that switching between electron and positron beams in DORIS could be accomplished in about one hour.

With sufficient luminosity and appropriate control of systematic uncertainties, a storage ring experiment with both electrons and positrons incident on an internal hydrogen gas target is the best way to measure the e^+p/e^-p cross section ratio. Simultaneous measurement both at low and at high ϵ with a large-acceptance detector configuration (BLAST) will allow a determination of the ϵ-dependence of the cross section ratio, and hence the size of the multiple photon contribution. Measurement at different beam energies will also enable a Rosenbluth separation for the positron cross sections for a wide range of four-momentum transfer when the measured e^+p/e^-p ratios are combined with existing Rosenbluth data for elastic electron-proton scattering.

1.4.1 Detector

We propose to utilize the existing Bates Large Acceptance Spectrometer Toroid (BLAST) detector system from MIT-Bates. BLAST is a toroidal spectrometer with eight sectors. The two horizontal sectors are instrumented with wire chambers for charged-particle tracking, plastic scintillators for trigger and relative timing, and aerogel-Cerenkov counters for pion rejection. The detector is symmetric about the beam direction and allows for complete reconstruction of coincident elastic events with both electron and proton four-vectors being determined. The symmetry of the detector doubles the solid angle for elastic scattering. The angle acceptance covers approximately $20°$ to $80°$ of the polar and $\pm 15°$ for the azimuthal angle.

The kinematic coverage of the BLAST detector is shown in Figure 1.6 for virtual photon polarization ϵ versus Q^2 for different incident beam energies (colors) and scattering angles (symbols) corresponding to the BLAST acceptance. For any given beam energy, the parameters ϵ and Q^2 are kinematically correlated within the large angle acceptance. For the BLAST detector geometry, the acceptance becomes smaller at higher beam energies, thereby setting a lower limit for the reachable value of ϵ since for backward lepton scattering angles the scattered proton is recoiling at decreasing angles and eventually misses the detector system. For the acceptance limitation by BLAST a proton angle $\theta_p > 23°$ was assumed.

As a consequence, the lowest reachable values of ϵ are about 0.4 and are only established at a beam energy of less than 2.3 GeV. At the same time, the beam energy should also not be smaller than 2 GeV in order to maintain a $Q^2 > 2$ $(\text{GeV/c})^2$.

For a fixed Q^2 of 2.6 $(\text{GeV/c})^2$ (where the $G_E(e^+)$ node is expected), only beam energies of 2.3-4.5 GeV are appropriate for use with BLAST. At this value of Q^2 the BLAST acceptances for these beam energies are overlapping, suitable to map out the ϵ-dependence of the cross section ratio at fixed Q^2 (similar to a Rosenbluth separation). The lowest beam energy corresponds to the lowest ϵ value for that respective Q^2 value. In combination with existing electron-proton cross sections, a Rosenbluth separation of the positron-proton elastic cross
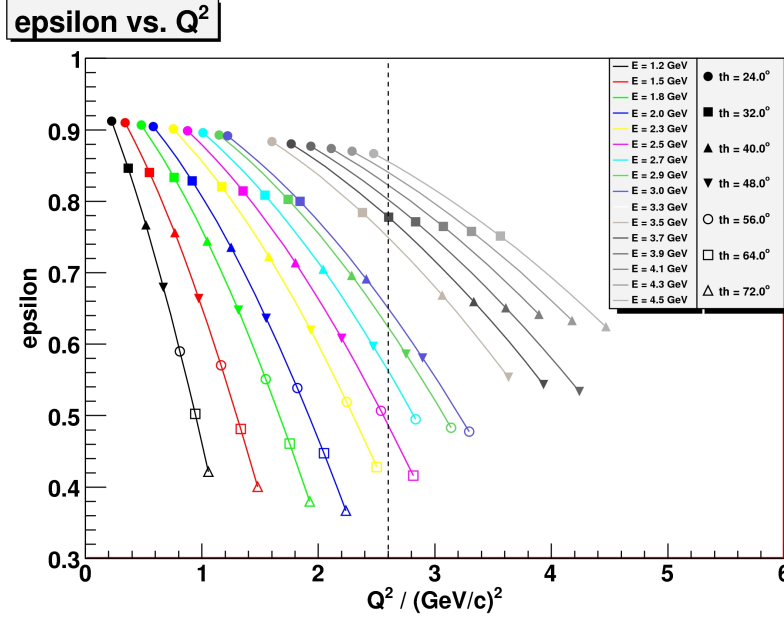
Figure 1.6: Kinematic coverage of ϵ versus Q^2 for the BLAST detector for various beam energies.

section can be carried out.

1.4.2 Target

The target will be an unpolarized hydrogen gas target confined by a thin walled, cryogenically cooled aluminum tube, similar to that used in the HERMES/DESY and BLAST/MIT experiments. To carry out measurements of the elastic electron-proton cross section at the lowest value of $\epsilon \approx 0.4$ with $\approx 1\%$ statistical uncertainty in about 1 month, a luminosity of $2 \cdot 10^{33}/(\text{cm}^2\text{s})$ will be required for this experiment. Assuming 100 mA circulating electron and positron currents, this implies a target thickness of about $3 \cdot 10^{15}$ atoms/cm². Large vacuum pumps will be required to pump away the hydrogen gas so that the lifetime of the stored beam can be on the order of several hours. The Erlangen, Ferrara, and MIT groups have considerable experience in designing, installing and operating such internal gas targets in storage rings [34].

We can estimate the beam lifetime in DORIS based on a simple model for losses accounting for bremsstrahlung, Møller and Rutherford scattering [36]. The current aperture at DORIS is limited by an undulator with an 11 mm gap, allowing only for a vertical emittance of about 7 mm-mrad. The momentum acceptance of DORIS (or bucket size) is estimated with 0.8%. The lifetime without any target in the current operation mode as a light source is on the order of 20 h. Figure 1.7 shows the expected partial lifetimes due to the various above mentioned processes that are causing losses, along with the resulting lifetime. It is assumed that the insertion of a target cell does not further limit the aperture. With a beta function sufficiently small at the location of the target, which can be achieved with a set of quadrupole magnets upstream and downstream of the internal target, this is a realistic as-
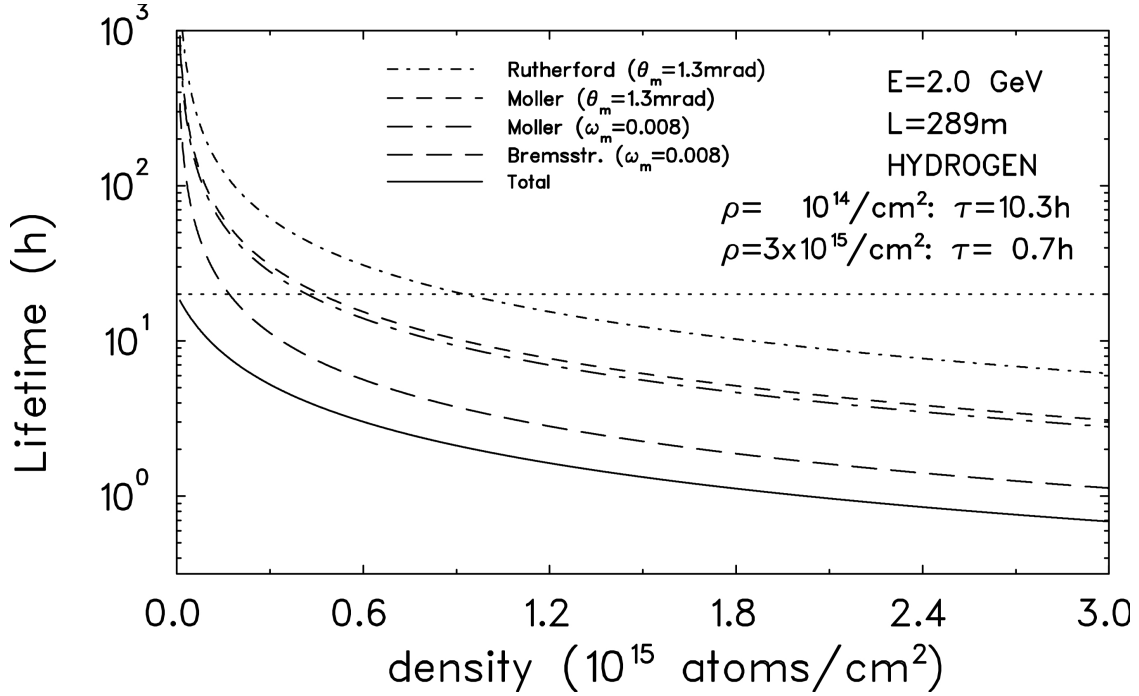
Figure 1.7: Expected beam lifetime in DORIS as a function of the target thickness. Based on a lifetime of 20 h without target (dotted line), the lifetime is reduced by Rutherford and Møller scattering and bremsstrahlung due to the given aperture limits (angle acceptance θ_m and momentum acceptance ω_m).

sumption. The expected lifetime at a beam energy of 2.0 GeV amounts to 10.3 h for a target thickness of 10^{14} atoms/cm^2 and 41 min for the required thickness of $3 \cdot 10^{15}$ atoms/cm^2. The momentum acceptance is still the dominant limitation. In comparison, the lifetime at MIT-Bates with a target thickness of $5 \cdot 10^{13}$ atoms/cm^2 was about 30 minutes.

1.4.3 Luminosity Monitor

The target thickness will be monitored over time by continuously measuring the pressure and temperature of the reservoir and by an additional flow meter to measure the flux from the buffer. The stored current of positrons and electrons in the ring will be measured with an absolute precision of 1% with a parametric current transformer as was done for BLAST running at MIT-Bates, providing a precise monitor of the luminosity when combined with the gas flow information from the buffer system.

Besides measuring target thickness and beam current separately, we also propose to measure and monitor the luminosity with elastic scattering at low momentum transfer. At low $Q^2 < 1$ (GeV/c)^2, the proton form factors G_E and G_M are known to the 1% level. Moreover, at ϵ close to 1, two-photon effects are expected to be negligible, hence the rate for both e^+p and e^-p elastic scattering is proportional to the luminosity. Since this experiment aims to precisely measure the ratio of elastic cross sections with positrons and electrons scattered from protons, only the relative or ratio of luminosities needs to be known with high precision.

To this extent, we will use a set of position-sensitive counters at a forward angle of about 10° to detect electrons or positrons in coincidence with the recoiling proton at large angle covered by the acceptance of BLAST. A schematic view of the proposed setup is shown in Fig. 1.8. At such a forward angle, the field integral of the BLAST toroid is quite
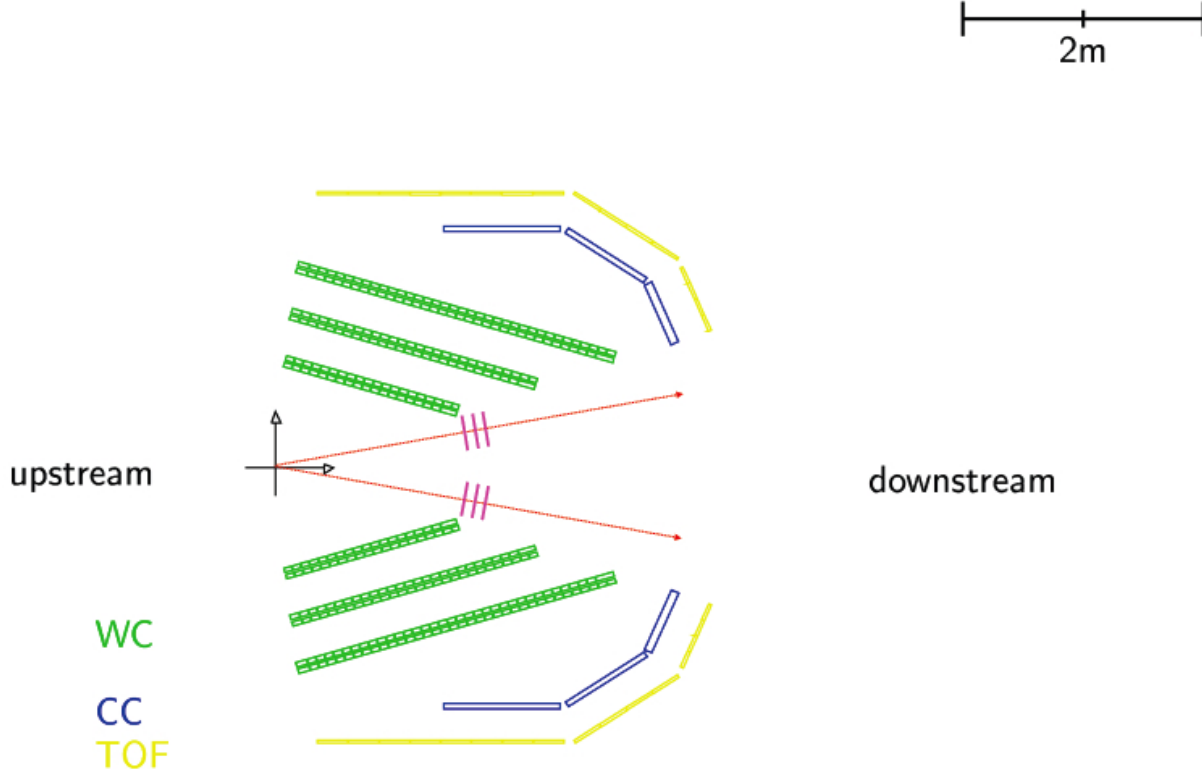

Figure 1.8: Schematic layout of the forward (10°) GEM telescope luminosity monitors.

small, resulting in almost straight tracks for elastically scattered electrons or positrons. The forward-angle detector will have to be radiation-hard, capable of handling high rates in the MHz region and has to provide good angular ($< 0.5°$) and vertex resolution (< 1 cm) for the forward tracks.

Our proposed solution for the forward detector will be a package of three planar triple-GEM detectors built as a tracking telescope, similar to the COMPASS-GEM [37] and the MIT prototype [38], allowing the lepton tracks to be measured with high resolution. Figure 1.9 shows the MIT prototype prepared for a test experiment at Fermilab [38]. The active area of the telescope will be 10×10 cm^2. Positioned at a distance of ≈ 160 cm from the target center, the solid angle will be 3.9 msr.

The coincidence requirement with the recoil proton in the BLAST detector provides redundant kinematic information to cleanly identify elastic scattering events. The elastic lepton track can be fully reconstructed back through the magnetic field to the target by inferring the lepton momentum from the proton track information. In addition, the azimuthal and polar angles as well as the measured time of flight can be correlated with the respective information of the proton.
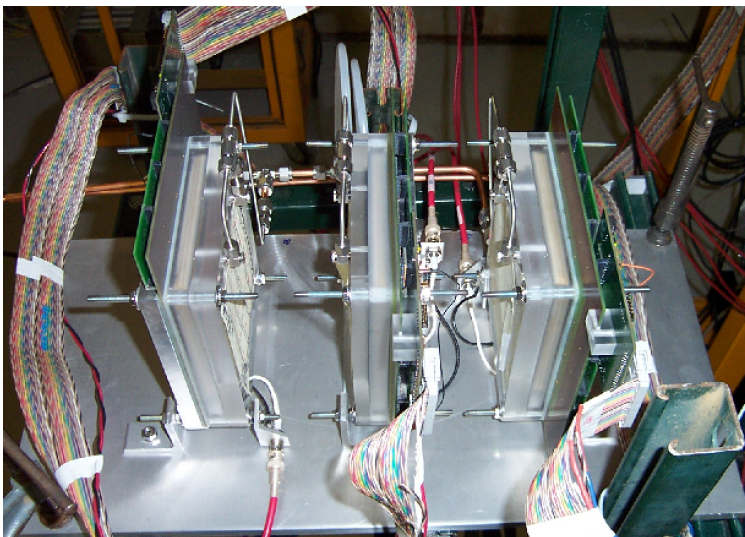
Figure 1.9: Triple-GEM tracking telescope for the test beam experiment at Fermilab.

For a point-like target, an alternative to a GEM tracking telescope could be several crossed layers of thin scintillator hodoscopes read out on both ends with fast photomultipliers for good position resolution. The angular resolution of the track should be better than 0.5°, which corresponds to a spatial resolution requirement of about 2 cm. While this modest requirement could already be achieved with a scintillator hodoscope, a higher resolution is required as also the vertex needs to be resolved as is the case for an extended target. With a typical spatial resolution of < 0.1 mm, the GEM telescope will provide vertex resolution of ≈ 1 cm, well matched to that of the proton reconstructed with BLAST.

For beam energies between 2.0 and 4.5 GeV, the four-momentum transfer at $\theta_e = 10°$ varies between 0.12 and 0.57 $(\text{GeV/c})^2$, and the virtual photon polarization parameter ϵ is above 0.98. Here the single photon approximation is good to better than 1%. The proton is recoiling with momenta of 350-820 MeV/c at angles of 63°–75°, well within the rear-angle acceptance of the BLAST detector.

The coincidence requirement between the forward detector and BLAST, as well as further kinematic correlations between the lepton and proton track, will suppress backgrounds from any source including random coincidences.

1.5 The Proposed Measurements

1.5.1 Luminosity monitoring

The cross section at low Q^2 and $\epsilon > 0.98$ is large enough to provide $< 1\%$ statistical error for the above configuration in less than one hour, indicating the suitability of this setup as a luminosity monitor. The expected count rate for this luminosity monitor is listed for beam energies of 4.5 and 2.0 GeV in Table 1.1.

E_0	Q^2	$p_{e'}$	ϵ	θ_p	p_p	Rate
[GeV]	[(GeV/c)^2]	[GeV/c]			[MeV/c]	[h^{-1}]
4.5	0.574	4.194	0.9825	63.1°	816	21286
2.0	0.118	1.937	0.9844	74.7°	349	402173

Table 1.1: Kinematics and count rates of the luminosity control measurement for beam energies of 2.0 and 4.5 GeV at $\theta_e = 10°$. The assumed solid angle is 3.9 msr.

1.5.2 Count Rate Estimate

Figure 1.10 shows the expected number of counts in any given angle bin and for various
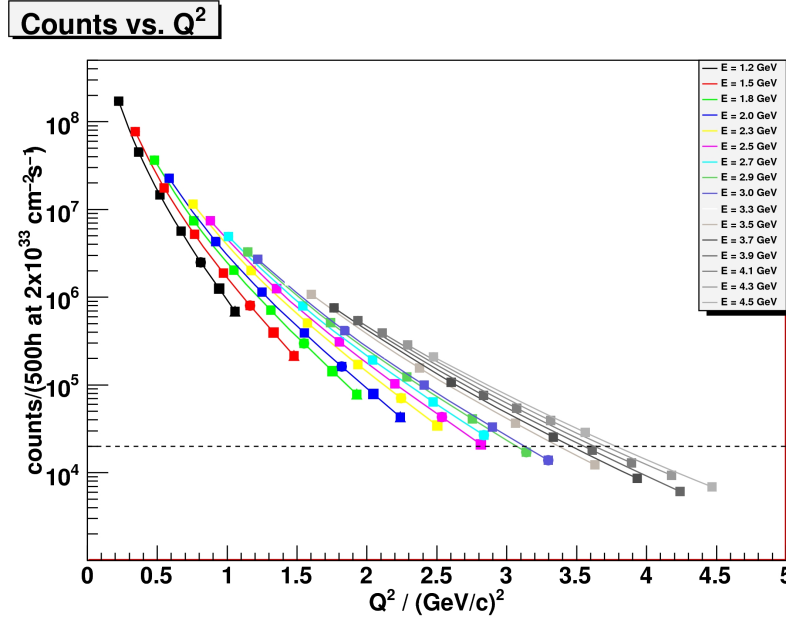

Figure 1.10: Expected distribution of counts per marked angle bin for the BLAST detector for various beam energies, as a function of Q^2. The assumed luminosity is $2 \cdot 10^{33}/(\mathrm{cm}^2 \mathrm{s}) \times$ 500 hours.

beam energies for a canonical run of 500 h at a luminosity of $2 \cdot 10^{33}/(\mathrm{cm}^2 \mathrm{s})$ as a function of Q^2. Höhler form factor [39] based cross sections were used for this estimate, good to within 10% for both e^+ and e^- up to $Q^2 \approx 3$ (GeV/c)^2. We see that for $Q^2 \simeq 2.6$ (GeV/c)^2, the number of counts per angle bin ranges between $\approx 2 \cdot 10^4$ (at 2.3 (GeV/c)^2 and smallest ϵ) and $\approx 2 \cdot 10^5$ (at 4.5 (GeV/c)^2 and highest ϵ).

Figure 1.11 shows the expected number of counts in any given angle bin and for various beam energies versus ϵ. Generally, lowest ϵ values at reasonable counts of $> 2 \times 10^4$, as required to provide statistical errors of the cross section ratio of $< 1\%$, are possible down to $\epsilon \approx 0.4$, for which the beam energy should not exceed ≈ 2.5 GeV. At higher energies, the lowest value of ϵ reachable with the rearmost scattering angle increases due to the proton forward angle acceptance limit, while at the same time the count rate decreases. However, also for energies lower than 2.0 GeV, the lowest reachable value of ϵ tends to increase as well
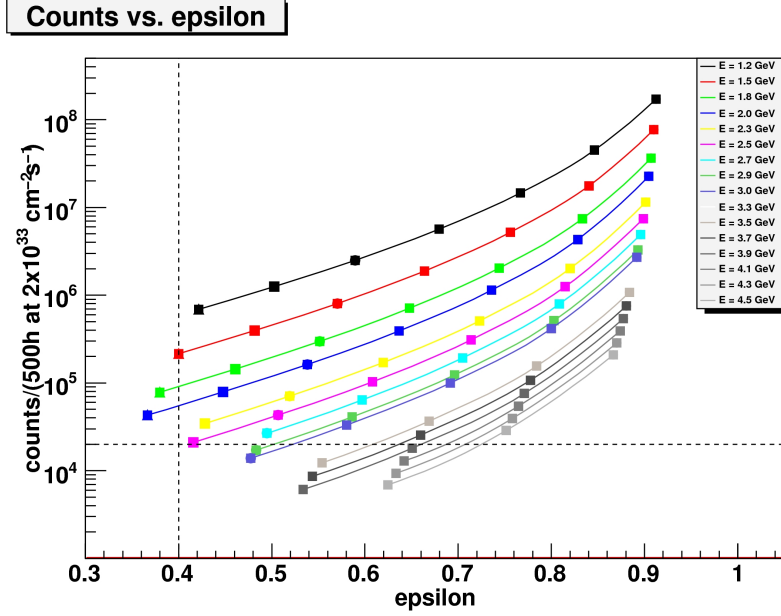
Figure 1.11: Expected distribution of counts per marked angle bin for the BLAST detector for various beam energies, as a function of ϵ. The assumed luminosity is $2 \cdot 10^{33}/(\mathrm{cm}^2\mathrm{s}) \times$ 500 hours.

E_0 [GeV]	Q^2 [(GeV/c)^2]	θ_e	$p_{e'}$ [GeV/c]	ϵ	θ_p	p_p [GeV/c]
4.5	2.6	24.9°	3.114	0.86	38.0°	2.125
3.0	2.6	43.0°	1.614	0.65	31.2°	2.125
2.3	2.6	67.6°	0.914	0.39	23.4°	2.125

Table 1.2: Kinematics for three beam energies and $Q^2 = 2.6$ (GeV/c)^2.

due the lepton's rear angle acceptance limit. A beam energy of 2.0 GeV appears to be ideal for the configuration of the BLAST detector to maximize count rate, acceptance and reach in ϵ.

Measurements at three beam energies, as listed in Table 1.2, can yield precise ratios of e^+p and e^-p cross sections at $Q^2 = 2.6$ (GeV/c)^2 for a wide range of ϵ. The counts for each Q^2 point in the table are in excess of $\approx 2 \cdot 10^4$ counts. In combination with world electron-proton cross section data this would allow for a precise Rosenbluth separation of the elastic positron-proton cross section at a value of Q^2 where the node of G_E^p when probed with positrons is expected (viz. Fig. 1.4).

For this experiment, however, we propose to run only at one beam energy, 2.0 GeV, to optimize cost and effectiveness of the measurement. At $\epsilon = 0.37$ and $Q^2 = 2.2$ (GeV/c)^2, the effect on $\sigma(e^+/e^-)$ is expected to be of the order 5%. For a 1% statistical error of the cross section ratio, about $2 \cdot 10^4$ counts are required for both electron and positron measurements. For a 500 h measurement each with electron and positron beams, the cross section ratio will be determined statistically to better than 1% throughout the BLAST acceptance. In

E_0	θ_e	$p_{e'}$	θ_p	p_p	Q^2	ϵ	Counts
[GeV]		[GeV/c]		[GeV/c]	[(GeV/c)^2]		
2.0	24	1.69	56.4	2.45	0.6	0.905	22613100
	32	1.51	48.1	2.26	0.9	0.828	4321570
	40	1.46	41.3	2.07	1.2	0.736	1141960
	48	1.27	35.7	1.89	1.6	0.636	389822
	56	1.10	31.0	1.73	1.8	0.538	162355
	64	0.97	27.1	1.59	2.0	0.447	78744
	72	0.85	23.8	1.47	2.2	0.367	42954

Table 1.3: Kinematics for 2.0 GeV beam energy and count estimate per 8° bin for 500 h at $2 \cdot 10^{33}$ / (cm^{2}s).

particular, the precision in the low-ϵ region for Q^2 up to 2.2 (GeV/c)^2 will not be limited by statistics.

It should be emphasized that the large angular acceptance of BLAST includes a wide distribution of ϵ values in a single measurement. Table 1.3 summarizes kinematics and expected count rate per 8° angle bin for the proposed run at a beam energy of 2.0 GeV.

Figure 1.12 shows the projected uncertainties, assuming a luminosity of $2 \cdot 10^{33}$ /(cm^{2}s) and a running time of 500 h for both e$^+$ and e$^-$. The theory curve is evaluated for constant beam energy as a function of ϵ.
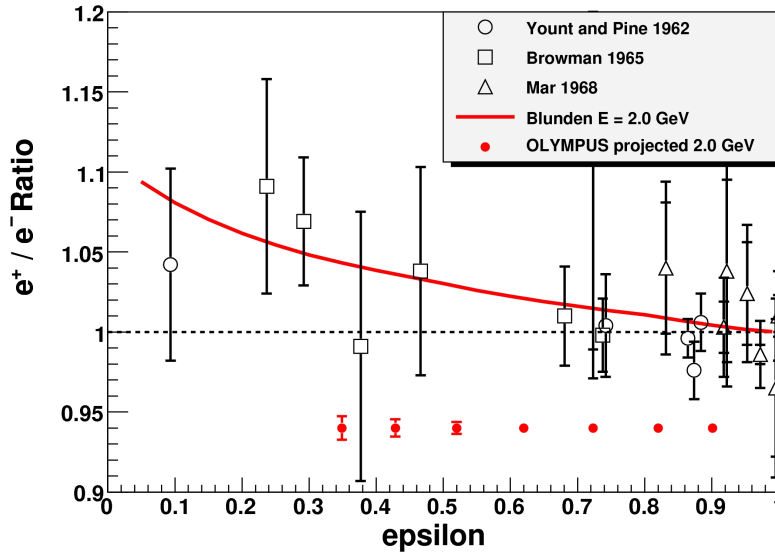

Figure 1.12: Projected uncertainties in the determination of the cross section ratio e^+p/e^-p for the BLAST detector for a beam energy of 2.0 GeV, as a function of ϵ. The assumed luminosity is $2 \cdot 10^{33}$ /(cm ^{2}s) $\times$ 500 hours each for running with electrons and positrons, respectively.

19

1.5.3 Control of Systematics

The primary observable of this experiment is the ratio of the electron-proton and positron-proton elastic cross sections. The redundant control measurements of the luminosity will allow the e^+p/e^-p cross section ratio to be determined with high precision. As shown below, the systematic errors for individual proton and lepton acceptance and efficiency will cancel to first order.

In order to reduce the systematic errors of the cross section ratio due to uncertainties in relative luminosity, acceptance and efficiency with individual electron and positron beams, we require that the beam in DORIS be alternated between electrons and positrons, and that the BLAST magnet polarity be reversed with the same frequency.

For a given angular bin, the number of events is given by

$$N_{ij} = L_{ij}\sigma_i \kappa^p_{ij} \kappa^l_{ij} \ , \tag{1.2}$$

where $i = e^+(e^-)$ for positrons (electrons) and $j = +(-)$ for positive (negative) BLAST magnetic field polarity, L is the luminosity, σ the bin-averaged lepton-nucleon cross section, and κ^p and κ^l are the geometric efficiencies for detecting the recoil protons and scattered leptons, accounting for the BLAST acceptance and detection efficiency.

With a given polarity of the BLAST magnetic field, the acceptance and efficiency for detecting the recoil protons will be identical for both electron and positron scattering, namely: $\kappa^p_{e^++} = \kappa^p_{e^-+}$ and $\kappa^p_{e^+-} = \kappa^p_{e^--}$. Hence, for a given field polarity, j , the proton efficiencies κ^p_{ij} cancel in the ratio

$$\frac{N_{e^+j}/L_{e^+j}}{N_{e^-j}/L_{e^-j}} = \frac{\sigma_{e^+}}{\sigma_{e^-}} \cdot \frac{\kappa^l_{e^+j}}{\kappa^l_{e^-j}} \ . \tag{1.3}$$

However, the acceptance and efficiencies for detecting the scattered electron or positron may differ for a given BLAST magnet polarity but will be the same for opposite polarities, namely: $\kappa^l_{e^++} = \kappa^l_{e^--}$ and $\kappa^l_{e^+-} = \kappa^l_{e^-+}$. By taking the product of the above ratio for opposite magnetic field polarities yields

$$\left[\frac{N_{e^++}/L_{e^++}}{N_{e^-+}/L_{e^-+}} \cdot \frac{N_{e^+-}/L_{e^+-}}{N_{e^--}/L_{e^--}} \right]^{\frac{1}{2}} = \frac{\sigma_{e^+}}{\sigma_{e^-}} \ , \tag{1.4}$$

which measures the cross section ratio directly where all lepton and proton acceptances and efficiencies cancel to first order.

As Eq. 1.4 indicates, the relative luminosities in the form of ratios need to be known precisely for an accurate determination of the cross section ratio $\sigma_{e^+}/\sigma_{e^-}$. A similar consideration holds for the measurement and combination of the four luminosities, L_{ij}, where the respective geometric efficiencies cancel. In order to measure the relative luminosity, we propose to use elastic scattering at forward angle corresponding to small Q^2 and large ϵ where the effects of two-photon exchange are negligible. Subsequently, the cross section ratio $\sigma_{e^+}/\sigma_{e^-}$ becomes unity, and hence the forward-angle coincident elastic rates N^{fwd}_{ij} are directly proportional to the luminosities in each of the four states {ij}

$$\frac{N^{fwd}_{e^++}}{N^{fwd}_{e^-+}} \cdot \frac{N^{fwd}_{e^+-}}{N^{fwd}_{e^--}} = \frac{L_{e^++}}{L_{e^-+}} \cdot \frac{L_{e^+-}}{L_{e^--}} \ , \tag{1.5}$$

and hence

$$\frac{\sigma_{e^+}}{\sigma_{e^-}} = \left[\left(\frac{N_{e^++}}{N_{e^-+}} \cdot \frac{N_{e^+-}}{N_{e^--}} \right) \Big/ \left(\frac{N_{e^++}^{fwd}}{N_{e^-+}^{fwd}} \cdot \frac{N_{e^+-}^{fwd}}{N_{e^--}^{fwd}} \right) \right]^{\frac{1}{2}} . \tag{1.6}$$

The ratio of relative luminosities in Eq. (1.5) can be measured at sub-percent statistical errors in less than one hour. Thus, frequent and random filling with both e^+ and e^- beams and reversal of the BLAST field direction will minimize systematic uncertainties in the ratio from acceptance and efficiency differences as statistics are accumulated. The period for alternating beams and magnet polarities has to be short compared to the time over which effects due to detector performance, such as detection efficiencies, are likely to change. Within that time frame, target density and beam current fluctuations, however, are appropriately accounted for and will have no systematic effect. Some period on the order of one day would likely be sufficient. The systematic error of each super ratio measurement according to Eq. (1.6) can thus be reduced by the square root of the number of cycles through the four states $\{ij\}$. E.g. for three months of running and by cycling through the four states once per day, the initial systematic uncertainty of the cross section ratio can be up to 9% in order to assure resulting systematic uncertainties of $< 1\%$, as a very conservative estimate.

Note the above derivation applies to the lepton detected in one sector of the BLAST detector and the proton detected in the opposite sector. During running data will be collected simultaneously for leptons and protons detected in both sectors yielding another level of redundancy and cancellation of systematic effects.

The above scheme makes use of measurements of the proton and lepton tracks in coincidence. Further information and additional checks of systematics will be obtained from proton or lepton single-arm events for which the high and low ϵ limits of the BLAST acceptance are extended. Provided that backgrounds in single-arm elastic events can be kept at a minimum, proton single-arm ratios for electron and positron beams with the same polarity of BLAST, as well as lepton single-arm ratios with reversed field polarity also probe the e^+/e^- cross section ratio independently.

1.6 Other experiments with similar goals

There have been proposals of two other experiments which aim to measure the positron-proton to electron-proton elastic scattering ratio, one at Jefferson Lab [30] using a secondary electron/positron beam from a pair production target, and another at Novosibirsk [31] based on stored electron and positron beams incident on an internal unpolarized hydrogen target.

1.6.1 Jefferson Lab

Experiment PR04-116 at Jefferson Lab [30] is prepared in Hall B using the CLAS detector. The setup of this experiment is shown schematically in Fig. 1.13 (l.h.s.). Since Jefferson Lab can not routinely provide positron beams, an effort is made to produce positrons as a secondary beam along with the electrons from a pair production target. The CEBAF electron beam of 1 μA and 5.7 GeV is converted into a photon beam at the bremstarget. The
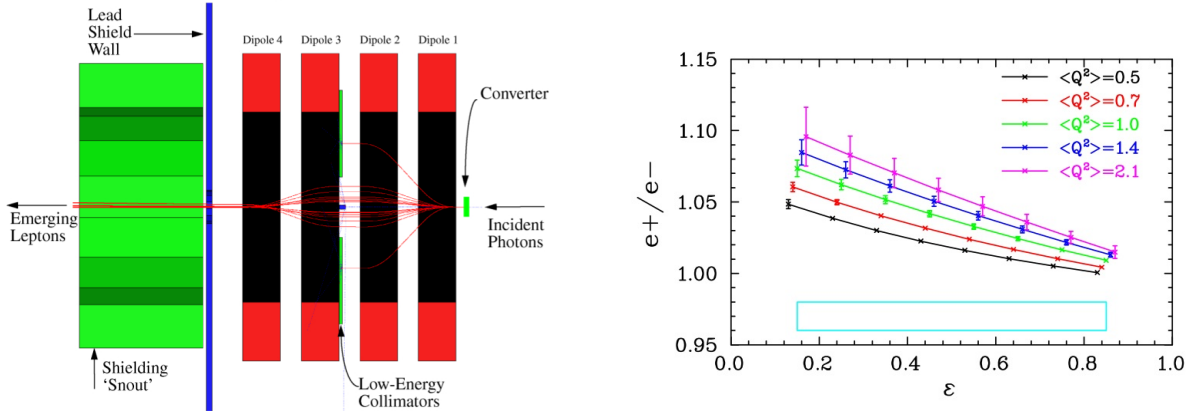
Figure 1.13: Left hand side: Schematic layout of secondary beam production for experiment PR04-116 at Jefferson Lab. Right hand side: Projected uncertainties with PR04-116 (Figures from [30])

.

photon beam then creates electron-positron pairs on a pair production target. A magnetic chicane separates and reemerges, and marks the energy of the electron and positron of each pair before they are steered onto the actual production target given by a 20 cm long liquid hydrogen cell. The elastically scattered leptons and recoil protons are detected by the CLAS detector. The initial electron beam of 1 μA would correspond to a current of 250 pA for the electron-positron pairs. In combination with the thick hydrogen target, the goal luminosity is 1.3×10^{33} /(cm^{2}s), somewhat below the design luminosity of OLYMPUS. Since the energies of the electron-positron pairs will by continuous, the measurement covers a range of Q^2 and ϵ in a single run. The projected results for the cross section ratio are shown in Fig. 1.13 (r.h.s.). The CLAS experiment reaches low ϵ of < 0.4 at values of Q^2 slightly above 2 (GeV/c)^2 with similar statistical precision as OLYMPUS in 35 PAC days.

A major challenge of PR04-116 is the production of the secondary beam in front of a large-acceptance detector, and the control of backgrounds associated with it. Extensive shielding along with eventual running of a modified mini-toroid to clean the beam will be required. Operating CLAS at 1 μA primary current, which is significantly higher than at standard operations, is a further challenge. However, an engineering run was carried out in 2005 with promising results. The experiment is currently scheduled to run in the final phase of the 6 GeV program at Jefferson Lab, before the shutdown for the 12 GeV upgrade, presumably in 2012.

1.6.2 Novosibirsk

The other proposed experiment aims to use the stored lepton beams at the VEPP-3 storage ring in Novosibirsk [31] along with an unpolarized internal hydrogen target. At first sight, this experiment has many similarities with OLYMPUS experiment. However, there are also clear distinctions between both approaches.

Most importantly, due to machine limitations, the maximum average current for stored positrons of this experiment will only be ≈ 9 mA; the target thickness of 10^{15} at/cm^2 will

be a factor 3 lower than in OLYMPUS, resulting in a luminosity for stored positrons of $\approx 5 \times 10^{31}$ / (cm²s), a factor 40 less than for OLYMPUS. The footprint of the detector setup to be used has similarities with the instrumentation of the BLAST detector, however it does not use any magnetic field. While in OLYMPUS the toroidal magnetic field serves both to provide tracking information and to clean off low-energy particles such as Møller electrons, the Novosibirsk experiment will have to deal with less redundancy in particle tracking and unavoidable background contributions from processes such as pion photo and electroproduction.

The setup as shown in Fig. 1.14 (l.h.s.) consists of small-angle (SA), medium-angle (MA) and large-angle (LA) sections, centered at 12°, 25° and 65°. The final data will be evaluated in a single bin for each section (20° wide for LA) to provide statistical uncertainty of better than 1%. The projected result is displayed in Fig. 1.14 (r.h.s.).
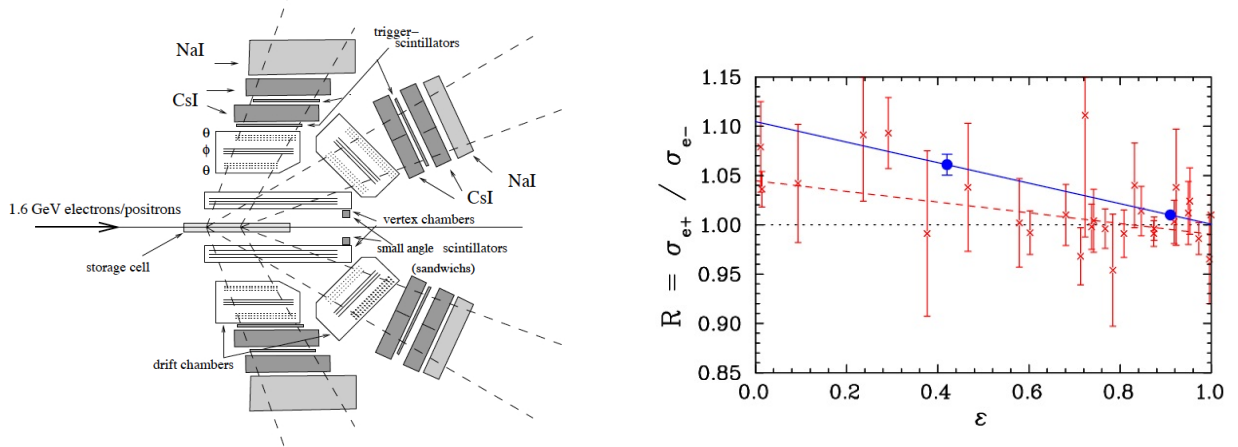

Figure 1.14: Left hand side: Schematic layout of the experiment at VEPP-3 in Novosibirsk. Right hand side: Projected uncertainties with this experiment (Figures from [31])

.

Similar to the proposed forward luminosity monitors in OLYMPUS, the forward detectors (SA) will be used for monitoring the luminosity; the MA section will provide a high-ϵ, and the LA section a low-ϵ point. The four-momentum transfer squared for the latter will reach $Q^2 \approx 1.5$ (GeV/c)^2 for a stored beam energy of 1.6 GeV, not quite as high as in OLYMPUS.

In comparison to both above proposals, the proposed OLYMPUS experiment is superior. While OLYMPUS provides the highest luminosity, it also offers the cleanest way of identifying elastic events. In contrary to both the CLAS and VEPP-3 experiments, OLYMPUS will essentially be a background-free measurement with respect to the final event sample selected.

This altogether will make OLYMPUS the definitive measurement to verify the two-photon exchange hypothesis.

Chapter 2

Details of the Experiment

2.1 Impact on the DORIS Ring

In this section, the modifications to the DORIS ring necessary to carry out the OLYMPUS experiment are described.

2.1.1 Required beam characteristics

The OLYMPUS experiment requires 100 mA of electrons and positrons incident on an internal hydrogen gas target of thickness 3×10^{15} atoms/cm^2 at an energy of 2.0 GeV. The lifetime of the stored beam is about 1 hour under these conditions. It is required to reverse the charge of the stored beam on a time scale of about 1 hour.

While the OLYMPUS data can only be taken in dedicated running, it is anticipated to commission the experiment in parallel with light source operation at the top energy of 4.5 GeV. Thus, F. Brinker (DESY) has developed a new optics for DORIS which provides a low beta waist at the location of OLYMPUS and leaves the stored beam characteristics essentially unchanged in the arcs. Figure 2.1 summarizes the beam characteristics and shows the horizontal (black) and vertical (red) beta-functions as calculated for the new optics using the MAD code.

The limiting apertures in DORIS together with the values of the beta-functions at the waist define the dimensions of the target storage cell. The limiting apertures are provided by the wiggler BW1 (vertical) and an absorber for Harwi (horizontal). The resulting target cell dimensions (full width) are 30 (horizontal) $\times$ 8 (vertical) mm^2. The target cell will be 600 mm in length as for BLAST. There will be a fixed collimator in front of the target cell to minimize scattering from beam halo.

2.1.2 Modifications to the DORIS Ring

It is proposed to install the OLYMPUS experiment at the location of the ARGUS experiment. This will require the following:

- Modification of the DORIS beamline and vacuum system in the vicinity of ARGUS to accommodate a beam waist at the location of the OLYMPUS internal gas target. This
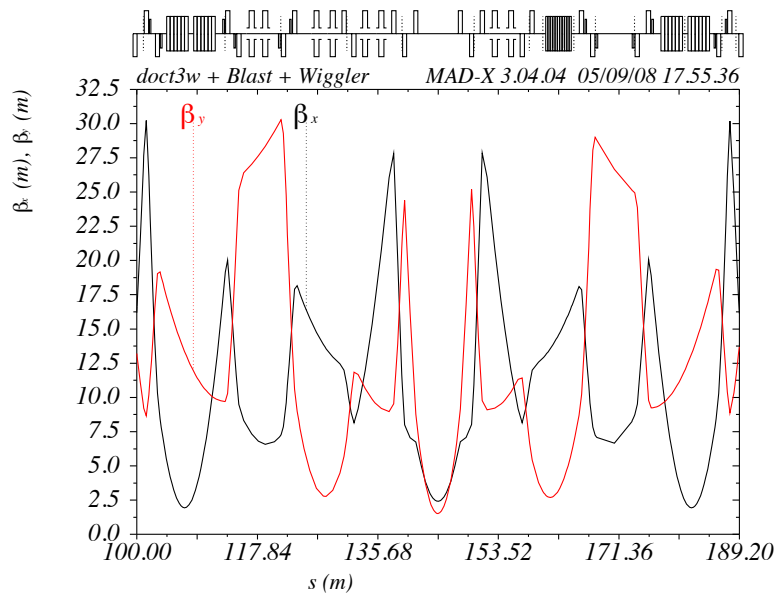
Figure 2.1: The new DORIS optics for the OLYMPUS experiment.

will entail moving 2 cavities to SL 26 m. In addition, two new quadrupole magnets together with a power supply are required. Finally, the OLYMPUS internal target system will be installed. A collimation system consisting of a fixed collimator directly in front of the target cell and movable collimators in the ring will be needed to minimize beam halo scattering from the target cell. These modifications can be accomplished during a scheduled shutdown of DORIS.

- Removal of the ARGUS detector, modification of the supports and rails, and installation of the BLAST detector. This can all be accomplished without a shutdown of DORIS.

- Installation of DORIS power supply polarity switches required for fast switching between positrons and electrons. This can be carried out during a scheduled shutdown of DORIS.

Radiation losses have been considered for OLYMPUS under the running conditions of the experiment and no unusual procedures have to be implemented beyond the standard shielding and safety protocols.

2.1.3 OLYMPUS Installation, commissioning, and data taking

The BLAST spectrometer and detectors can be installed at the site of the ARGUS detector in parallel with DORIS operation. The installation of the OLYMPUS experiment can occur during scheduled shutdown periods of DORIS and in parallel with DORIS operation. The modification of the DORIS beamline and the installation of the OLYMPUS internal gas target will require a shutdown of the ring.

Wiggler	β_x		α_x		β_z		α_z	
	doct3w	Blast	doct3w	Blast	doct3w	Blast	doct3w	Blast
BW1	18.23	17.98	-1.07	-1.04	3.95	4.02	0.398	0.459
BW2	8.69	8.55	-0.038	-0.050	16.19	15.73	-0.022	-0.068
BW3	22.52	22.70	-0.014	-0.033	5.35	5.65	-0.120	-0.133
BW4	0.72	0.71	-0.010	0	6.58	6.41	0.027	0.074
BW5	22.30	22.74	0.037	0.036	50.3	4.94	0.148	0.093
BW6	8.46	8.54	0.033	0.051	15.09	15.90	-0.012	0.004
BW7	18.22	17.92	1.04	1.037	4.17	3.95	-0.451	-0.433
Harwi	12.88	14.56	-0.209	-0.459	4.04	3.21	0.266	-0.414
Roewi	4.78	3.75	0.021	-0.037	11.72	9.01	0.027	0.014
Blast IP	26.16	2.41	-0.022	-0.001	9.707	1.52	0.048	-0.026

	doct3w	doct3wBlast
Emittance	465 nm	438 nm
mom. compaction	0.0134	0.0138
Qx	7.17	7.17
Qz	4.77	5.23

Table 2.1: Comparison of optical functions at centre of wigglers - actual standard optic versus optic for Blast

It is proposed to begin commissioning of OLYMPUS with 4.5 GeV beam at greatly reduced target thickness (so that it does not affect the DORIS stored beam lifetime) in parallel with light source operation. It is anticipated that over a period of three months duration the experiment could be successfully commissioned at low luminosity at 4.5 GeV energy. Further, it is noted that some shifts of commissioning at higher gas thickness and lower beam energy should be possible during the regularly scheduled maintenance periods. Over a period of some months, the OLYMPUS experiment could be commissioned at full luminosity and proposed beam energy of 2.0 GeV.

To obtain the proposed results in Figure 1.12 will require 500 hours of data taking for each lepton sign at 2.0 GeV incident energy. Thus, a total of 1,000 hours of 100% efficient data taking is required. Assuming an efficiency of 50% for data taking, 2,000 hours or 3 months of dedicated DORIS operation at 2.0 GeV are requested for the OLYMPUS experiment. It is proposed that the 2,000 hours be delivered in two 1,000 hour blocks, not less than six months apart. The break will allow time for understanding the systematic uncertainties which will limit the total uncertainty in the experiment.

2.2   The BLAST spectrometer

The BLAST detector as it was configured at Bates is shown in Figure 2.3.

It was situated on the South Hall storage ring just downstream of the injection point. The detector was based upon an eight sector, toroidal, magnetic field. The two horizontal sectors were instrumented with detector components while the two vertical sectors were used
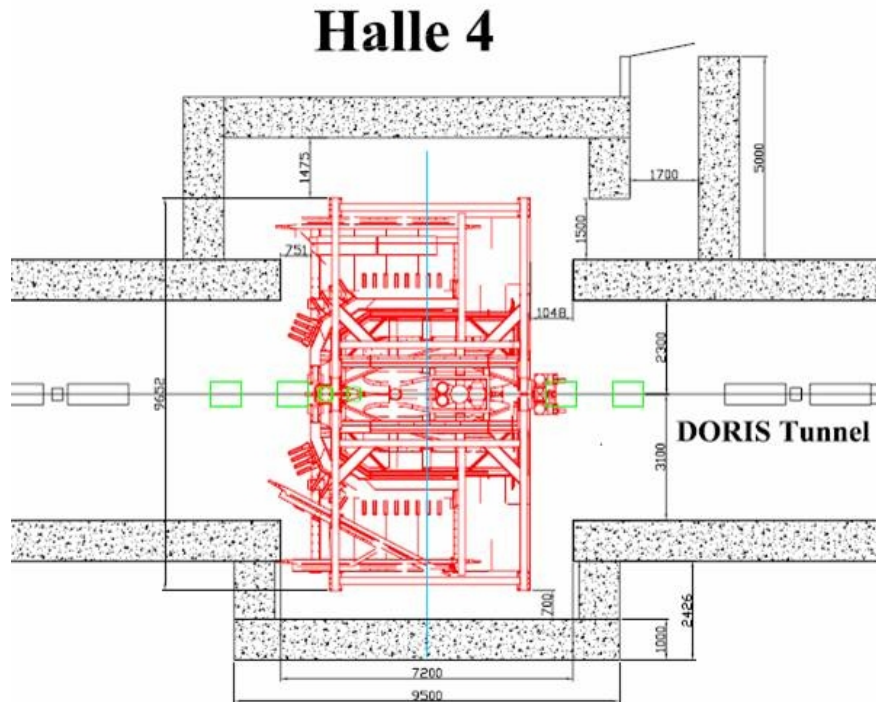
Figure 2.2: The BLAST detector at the location of the present ARGUS interaction point.

by the internal targets and pumping for the beamline.

The detector configuration we propose to use in OLYMPUS will use the BLAST toroidal magnet and instrument the horizontal sectors with the BLAST wire chambers and time of flight scintillators. As such the detector will be left/right symmetric. The drift chambers will provide charge particle tracking to determine the charge, momentum, scattering angles, and vertex for the charged particles produced. The time of flight scintillators will determine the relative timing of the reaction products and provide the trigger timing for the detector system.

In addition to the existing BLAST detector elements some new detector components and upgrades to the BLAST detectors are possible to improve the performance.

The following sections describe the detector components in greater detail.

2.2.1 Toroidal Magnet

The toroidal magnet was designed and assembled at MIT-Bates. A toroidal configuration was chosen to ensure a small field along the beamline to minimize effects on the beam transport and also to have small gradients in the region of the target cell. The magnetic field in the region of the drift chambers was used to momentum analyze the charged particles produced during the experiment. It also minimized the number of low energy charged particles reaching the detectors.

The toroid consisted of eight copper coils placed symmetrically about the beamline. Each coil consisted of 26 turns of hollow, 1.5 inch square copper tube organized into two layers
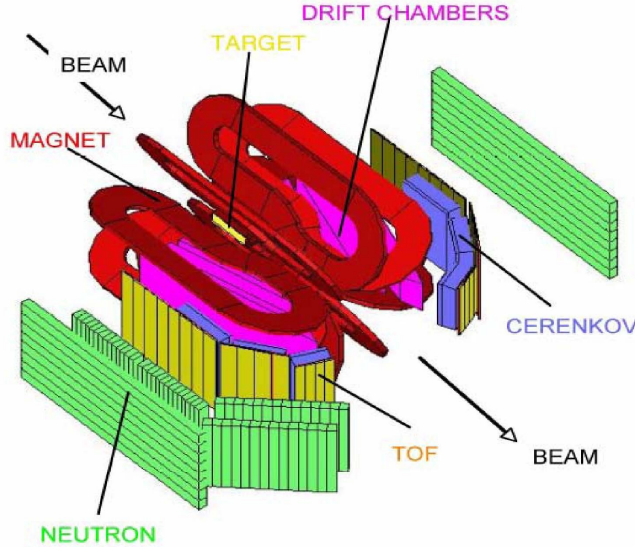
27

Figure 2.3: Schematic of the BLAST detector showing the main detector elements.

of 13 turns. The copper tubes were wrapped with a fiberglass tape and then potted with epoxy resin. The coils were cooled by flowing water through the hollow conductors. During the BLAST experiment the normal operating current was 6730 A resulting in a maximum field around 3.8 kG.

Before the detectors were installed, the magnetic field was carefully measured particularly along the beam axis and in the target region [40]. The coil positions were adjusted to minimize the field along the beamline and gradients at the target. After this was done a systematic mapping was performed of the magnetic field in each of the horizontal sectors throughout the volume which would be occupied by the tracking detector. The results of this mapping were compared with results from a simple calculation based on the Biot-Savart law as well as a Vector Fields TOSCA simulation. The agreement was reasonable.

Discrepancies between the measured and calculated field values could be explained by the uncertainty in the precise conductor positions and by the deflection of the coils under gravity or when energized. The Biot-Savart calculations were redone allowing the coil positions to move radially, along Z, and in azimuthal position to obtain good agreement with the measured values. These calculated values were then used to extend the mapping to regions where it was impossible to make a direct measurement. This extended mapping was used in the reconstruction of events.

Note: for the proposed OLYMPUS measurement precise knowledge of the magnetic field is not necessary as the measurement will be based on ratios of rates as discussed in section 1.5.3. Nevertheless, the initial alignment of the toroid to minimize the effect on the DORIS beams will be done. Also the field in the tracking volume will be measured at a number of points before the drift chambers are installed and the coil positions measured to provide data for comparison with Biot-Savart calculations which will be used to generate the

Figure 2.4: The eight coil BLAST toroid without its detectors.

magnetic field mapping using in tracking and momentum analysis.

2.2.2 Drift Chambers

The drift chambers shown in Figure 2.5 measured the momenta, charge, scattering angles, and vertices for the particles produced in the reactions studied with BLAST. This was done by tracking the charged particles in three dimensions through the toroidal magnetic field and reconstructing the trajectories. Measuring the curvature of the tracks yielded the particles' momenta, and the directions of curvature determined their charge. Tracing the particles' trajectories back to the target region allowed the scattering angles, polar and azimuthal, to be determined and the position of closest approach to the beam axis was taken as the vertex position for the event.

To maximize the active area, the drift chambers were designed to fit between the coils of the toroidal magnet such that the top and bottom plates of the drift chamber frame were in the shadow of the coils as viewed from the target. The drift chambers had a large acceptance and nominally subtended the polar angular range 20°–80° and ±15° in azimuth with respect to the horizontal and were positioned and orientated such that 73.54° with respect to the beam from the target center was perpendicular to the face of the chambers. Because of these choices the chambers were trapezoidal in shape (see Figure 2.6).

Each sector in BLAST contained three drift chambers (inner, middle, and outer) joined together by two interconnecting sections to form a single gas volume. This was done so that only a single entrance and exit window was required for the combined drift chambers thus minimizing energy loss and multiple scattering.

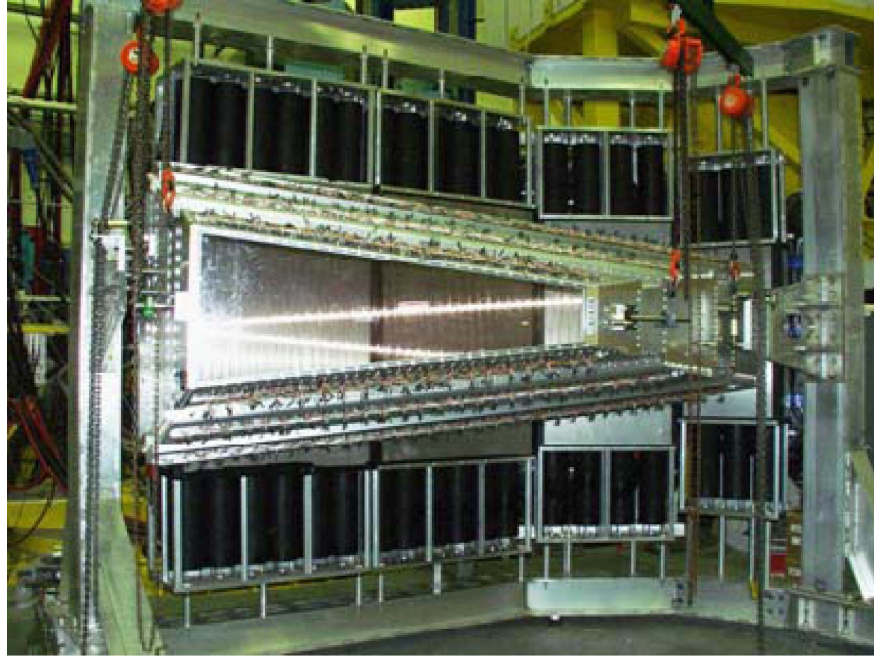Each chamber consisted of two super-layers (or rows) of drift cells. The drift cells were

Figure 2.5: Photo of the BLAST drift chambers mounted in the sub detector support frame in its rolled-out position.

"jet" style formed by wires. Figure 2.7 shows the wire pattern for a portion of one chamber. Each drift cell had 3 sense wires staggered ±0.5 mm from the center line of each cell to help resolve the left/right ambiguity in determining position from the drift time. This pattern of wires was realized by stringing wires between the top and bottom plates of each chamber. Holes for each wire were machined in the thin plate of the recessed areas of the top and bottom plates to accept Delrin feed-throughs. The feed-through had a gold plated copper tube insert through which the wire was strung and crimped. The pin provided a convenient connector for the HV.

The three drift chambers for a sector combined into a single unit were then mounted in the sub-detector frame and its position and orientation adjusted until it was in its nominal position. This position was checked by an optical survey and this data was used together with a previous survey and the data from the CMM data on the hole positions to determine the position of each sense wire in the BLAST coordinate system

With all three drift chambers assembled and positioned in each sector there were 18 planes of sense wires with which to track the charged particles produced at BLAST. In total there was approximately 10,000 wires with 954 sense wires for both sectors in BLAST.

A helium:iso-butane gas mixture (82.3:17.7) was chosen for the drift chambers. The chambers were maintained at a pressure of approximately 1 inch of water above atmospheric pressure with a flow rate of around 3 l/min. The primarily helium mixture has a relatively low density to reduce multiple scattering and energy loss. Also, because the BLAST toroidal field is inhomogeneous over the tracking volume, a small Lorentz angle is desirable so that corrections are small even in regions with high magnetic fields. The helium gas mixture chosen satisfies this as well with ≈ 7° Lorentz angle in a 3.8 kG field. Figure 2.8 shows the
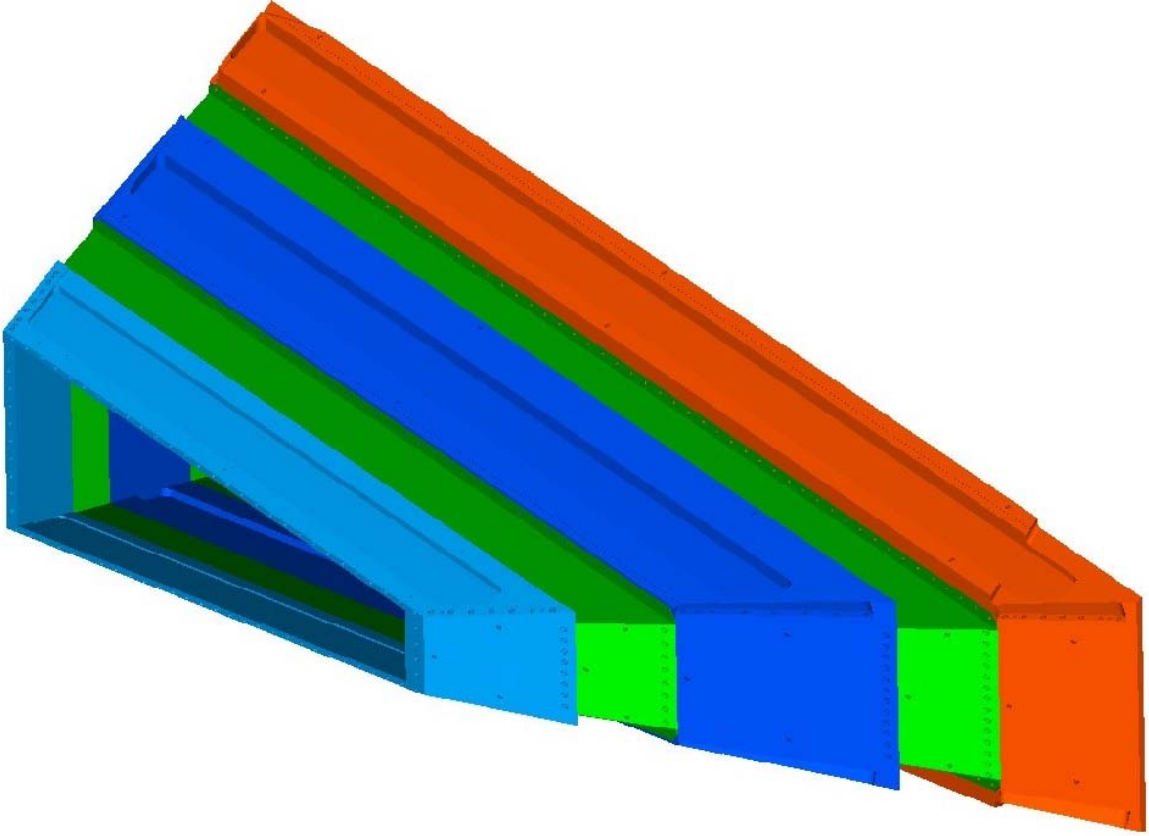
Figure 2.6: Isometric view of all three drift chambers assembled into a single gas volume.

distinctive lines of electron drift, "jets", for this cell design at 3.8 kG. Using a single gas volume minimizes the number of entrance and exit windows for the same reason. Two layers of 25 micron mylar were used for the entrance and exit windows.

2.2.3 Upgrade to Wire Chambers

Even with 18 planes of sense wires in the BLAST drift chambers there were times when more redundancy would have been useful. This was because the 6 sense wire planes in each of the three chambers in a sector were relatively close together and thus tended to yield a single point in space or at best a short track segment. Thus the track reconstruction had three points or track segments for each track with which to fit the momenta, scattering angles, charge and vertex. While this was possible there was no redundancy with which to get a measure of the accuracy of the reconstruction or to use the data to improve the track fitting parameters. Because of this we would like to add a triple GEM detector approximately 40 cm from the target in front of the wire chambers in both sectors.

This detector would be ~ 50 cm long and trapezoidal in shape varying from 12 to 48 cm in height to match acceptance of the wire chambers. The frames of these triple GEM detectors would be in front of the toroid coils so would not reduce the active area. A conservative
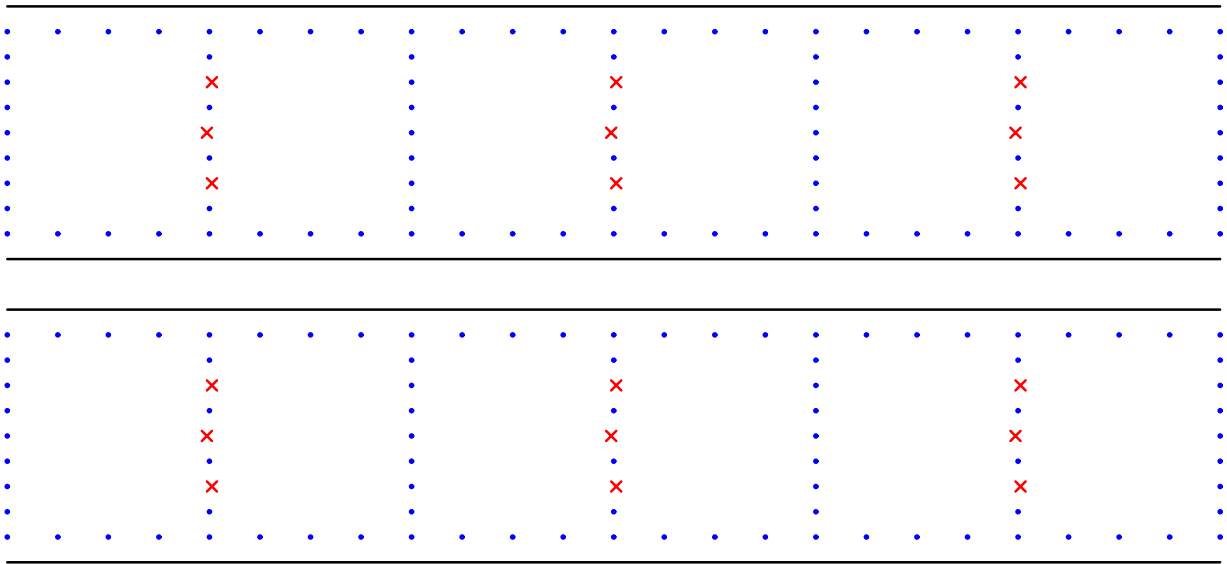
31

Figure 2.7: Schematic of wire layout in one chamber showing the drift cell pattern for both super-layers.

2D-readout design with 1 mm line pitch should give position resolutions on the order of 150 microns comparable to that of the wire chambers and require less than 1280 channels of readout.

The choice of GEM technology is based on the fact that GEM's are:

- thin - $< 0.7\%$ radiation length

- fast - can handle rates up to 500 kHz/cm^2

- 2D-readout can provide both X and Y information

- compact - approximately 10 mm thick

- accurate - resolutions better than 50 microns are possible

- radiation tolerant

- insensitive to magnetic fields

In addition we can benefit from an existing program at MIT which is producing large triple GEM detectors for an upgrade to the STAR forward tracking region. This would allow a shared common effort in producing large GEM foils, readout and control electronics, and quality assurance and testing.

A detailed design needs to be done based on the limits for manufacture of large GEM foils and the optimal position of this detector component. While GEM foils can handle very high rates it would be better if the Møller electrons could be swept away by the toroidal magnetic field.
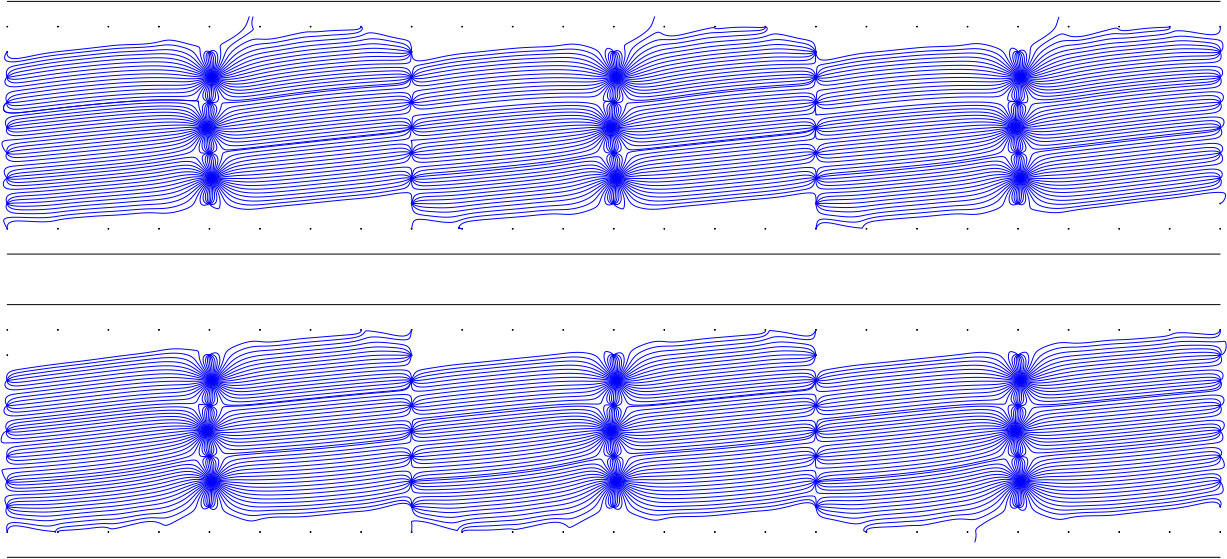
32

Figure 2.8: Lines of electron drift in the drift cells assuming the maximum BLAST field of 3.8 kG.

GEM Technology

A single Gas-Electron Multiplier (GEM) consists of a thin metal-clad insulation foil perforated by a regular dense hole pattern [41]. The holes in the foils typically have a double conical shape with an inner diameter of ~ 50 μm, an outer diameter of ~ 70 μm and a pitch of 140 μm. Figure 2.9 shows an electron microscope picture of a GEM foil and a cross
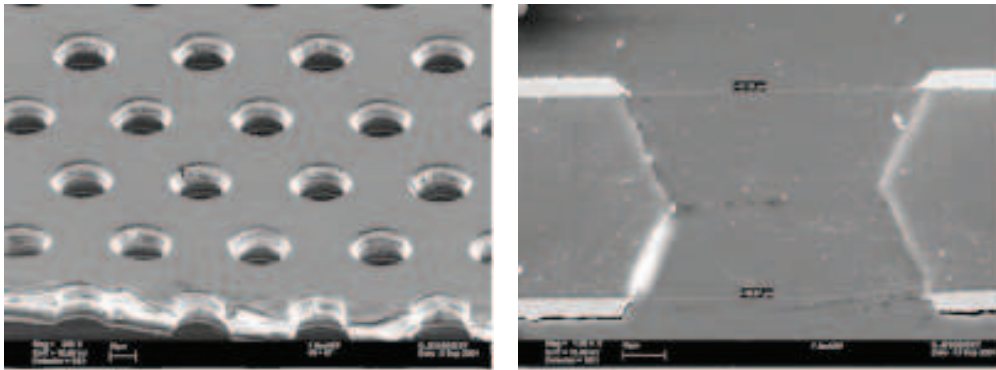

Figure 2.9: Electron microscope image of a GEM foil and cross sectional view of a GEM hole. [42].

section view of one hole.

A voltage difference between the two metal-clad sides of the foils leads to high electric fields in the holes, as illustrated in Figure 2.10. This is used to achieve electron multiplication in the detector gas.
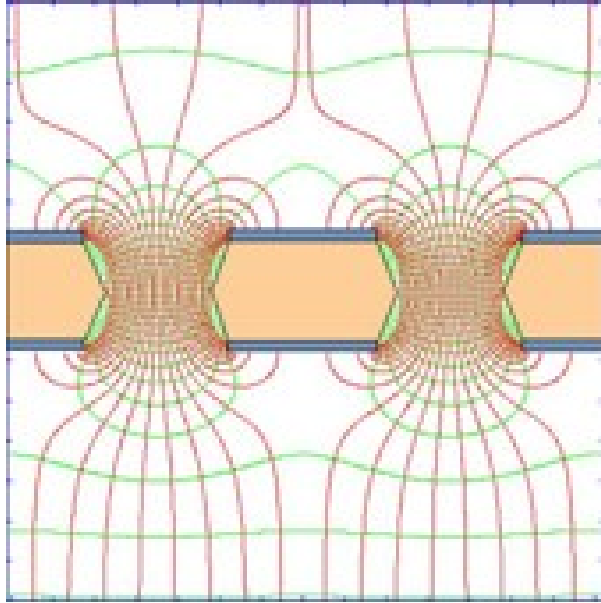
Figure 2.10: Simulated electrical field inside a GEM hole. Electrons released in the upper gas volume drift into the holes, multiply and get transferred to the lower side.

A triple GEM detector configuration is shown in Figure 2.11 charged particle ionizes the gas in the drift region above the first GEM foil. The applied electric field accelerates the electrons to the GEM foil and a significant fraction ($\sim 60\%$) enter the holes in the GEM foil where, due to the high electric fields, ionize the gas further resulting in a gas gain of 20–100. This process is repeated with the second and third GEM foils until finally the avalanche of electrons is detected on the readout plane. Gains up to 10^6 have been achieved though typically gains of 10^5 are sufficient for detection with current electronics.

In practice the top GEM foil is operated at higher gain and the last GEM foil at a lower gain to avoid breakdown because of the abundant charge in the region. The readout can be a single layer with pads or strips but a two dimensional readout is also possible by producing lines on both top and bottom surfaces of a thin foil and exposing the bottom lines by carefully removing the insulating material between the lines on the top surface either through etching or laser ablation.

2.2.4   Time-of-Flight Scintillators

In each sector 16 vertical scintillator bars formed the time-of-flight (TOF) detector. The TOF detector was designed and produced at the University of New Hampshire to provide a fast, stable timing signal correlated with the time of each event at the target independent of which scintillator bar was struck. This signal was used to trigger the readout and data acquisition system for all other components and particularly provided the COMMON STOP signal for the drift chambers. This permitted relative timings among all components to be measured. The TOF detector also provided a measure of energy deposition to aid particle identification. Approximate position information was also possible from the timing difference
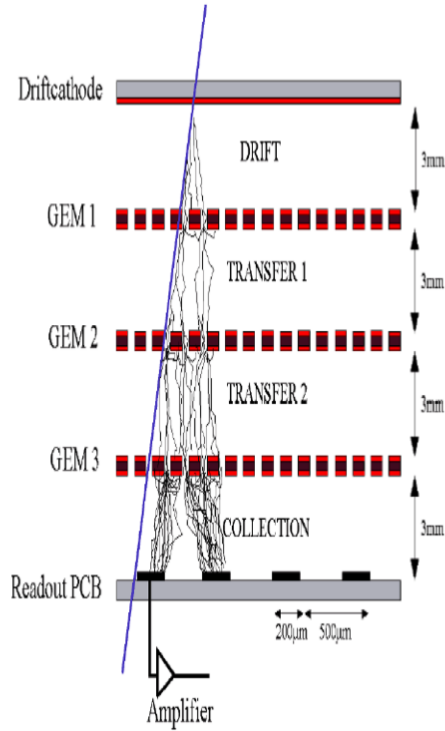
Figure 2.11: Schematic illustrating the concept of a triple GEM detector.

between the top and bottom photomultiplier tubes.

The TOF detector curved behind (see Figure 2.12) the wire chambers and Čerenkov detectors in each sector roughly matching the angular coverage of the tracking detector in both polar ($\sim 20° < \theta < \sim 80°$) and azimuthal ($\pm \sim 15°$) projections. The forward four bars at $\theta < 40°$ were 119.4 cm high, 15.2 cm wide, and 2.54 cm thick. The remaining 12 bars at $\theta > 40°$ were 180.0 cm high, 26.2 cm wide, and 2.54 cm thick.

Bicron BC-408 plastic scintillator was chosen for its fast response time (0.9 ns rise time) and long attenuation length (210 cm). Each TOF scintillator bar was read out at both ends via Lucite light guides coupled to 3 inch diameter, Electron Tubes[1] model 9822B02 photomultiplier tubes, PMTs, equipped with Electron Tubes EBA-01 bases. The light guides were bent to point away from the interaction region so the PMTs would be roughly perpendicular to the toroidal magnetic field. Mu-metal shielding was used around all PMTs. The bases have actively stabilized voltage dividers so that the timing is independent of the gain.

With readout from both ends of a TOF scintillator bar, the time difference provided coarse position information. To provide a timing signal independent of position along the TOF, the signals from each PMT were split, with one part from each pair of tubes going to a meantimer. This meantime signal was used to provide the event timing signal. Because each TOF was at a different distance from the target center, a delay was added to the closer detectors corresponding to the time for a relativistic particle to travel the difference in distance. These

---

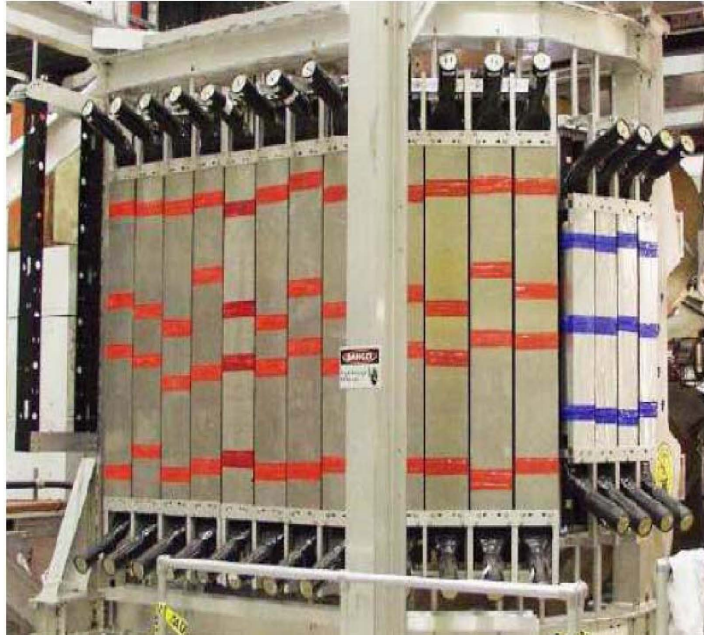[1]Electron Tubes Ltd, Bury Street, Ruislip, Middlesex, HA4 7TA, England

Figure 2.12: TOF detector mounted in sub-detector support during assembly.

time differences were measured for each sector by inserting a thin plastic scintillator paddle near the target chamber and measuring the TOF detector timing relative to the common start from this paddle. These delayed, mean-timed signals were thus correlated with the time of the event at the target. The signals from each PMT were also distributed to TDCs and ADCs.

A 2 mm thick lead foil was placed in front of each TOF bar to attenuate X-rays from the target region. It also prevented back-scattered radiation from firing the Čerenkov detector and being mis-identified as electrons. However, the lead foil was removed from the rear-most four TOF scintillator bars to improve the sensitivity to low energy deuterons.

Gains for the PMTs were set by requiring the ADC signal for minimum ionizing particles from cosmic rays to peak in channel 1250. A time resolution of 320 ± 44 ps was measured for the 32 TOF detectors which was significantly better than the 500 ps required by the experiment. Timing offsets between pairs of scintillator bars were determined using cosmic rays periodically during the experiment. The efficiency was determined to be better than 99%.

Figure 2.13 illustrates the performance of the TOF detector using elastic ep scattering. The large figure shows the coincidence between hits in a TOF detector in one sector versus the other. The line of peaks corresponds to elastic scattering kinematics. The empty plots illustrate how rare random coincidences were and how clean event selection was using just TOF timing information. The insets show the timing resolution and coplanarity for ep elastic scattering. The TOF timing resolution was typically around 400 ps. The vertical position of the TOF hit could be determined from the time difference between the top and bottom PMTs. Comparing the vertical position of TOF hits in left and right sectors for ep elastic scattering and requiring that the event originated in the target yielded a coplanarity
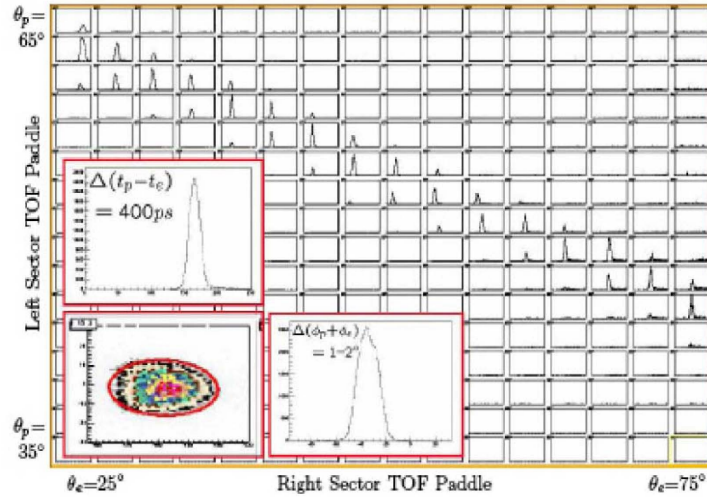
Figure 2.13: TOF timing results using *ep* elastic scattering. The large figure shows the coincidence between TOF counters in left sector versus those in the right sector for events where the trigger was generated by a hit in the right sector. The insets show the timing resolution and coplanarity of elastic *ep* scattering.

better than 2°. Thus TOF timing information was very important in event selection and significantly reduced the background.

2.2.5 Trigger and DAQ

The trigger will be built along the design that was used for the BLAST spectrometer at MIT/Bates, reusing existing modules.

The signals from the TOF scintillators are split to provide a fraction for the measurement of the energy deposition by an ADC, and to provide signals for time measurement and trigger purposes. The latter signals are discriminated using constant fraction discriminators, the coincidence signal of the top and bottom PMT of each scintillator is then generated and fed into a memory lookup table, that allows to logically combine the signals in arbitrary ways. The data from this memory lookup table is then combined with data from the other sector of BLAST, and so in a further lookup table the final trigger is formed, see figure 2.14.

The trigger signal then provides the gates and start signals to the ADCs and TDCs respectively, which digitize the information from the TOF scintillators and the drift chambers. Corresponding modules in the FASTBUS standard are available, they are read out via Fastbus/VME interface modules. For the new detector components, especially the GEMs, a special readout is required. In detail, it depends on the design of these components, it is therefore discussed in the corresponding sections.

For the readout software of the DAQ system several possibilities are explored, among
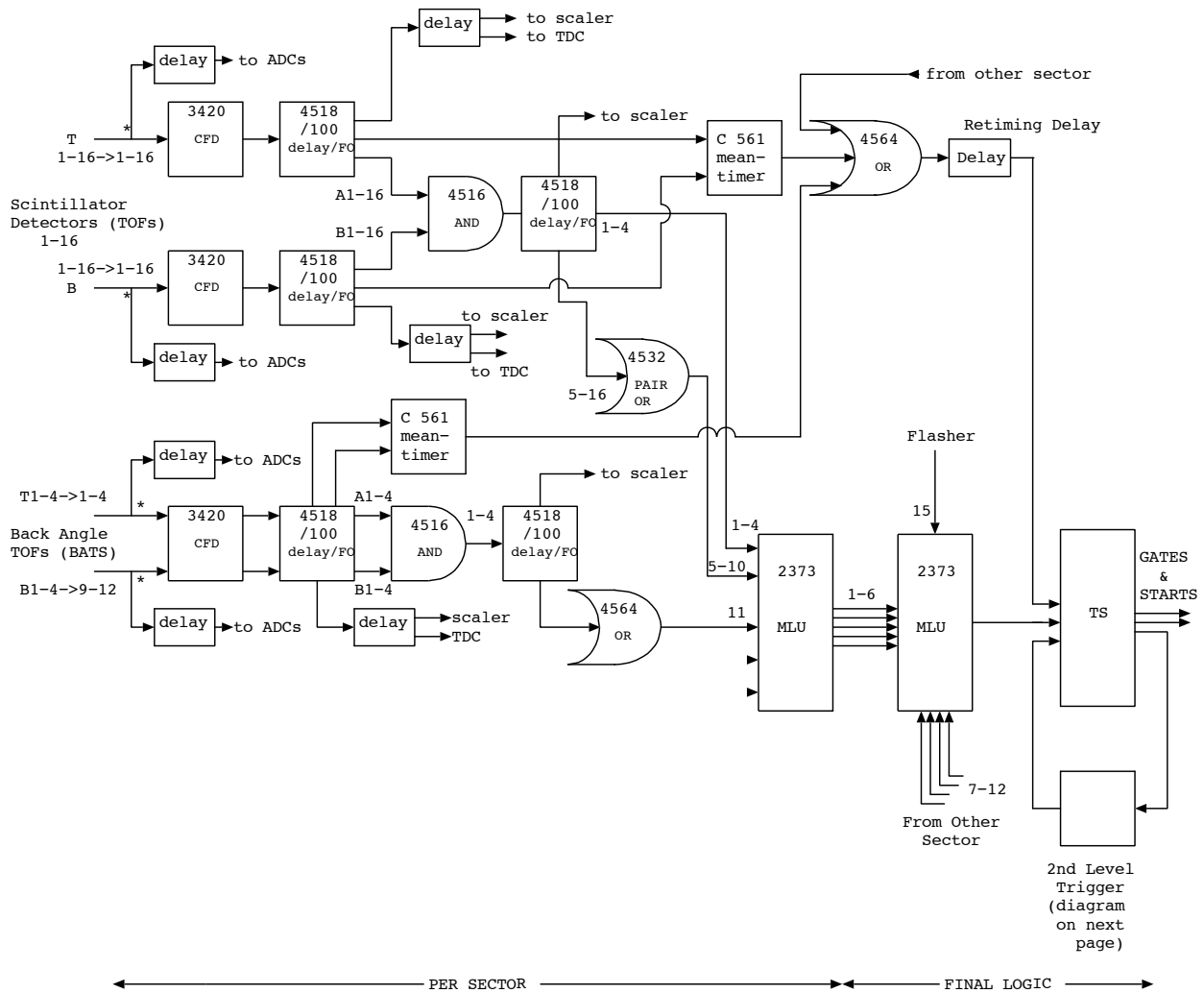
37

Figure 2.14: Trigger schematics

them CODA, the system that was used with BLAST in the past, or the software used in the CB/ELSA experiment at Bonn.

While it is possible to build the trigger and DAQ system almost completely from existing equipment, it is considered to replace a few key components by more modern parts. The MLUs of the trigger system could be replaced by a FPGA based board, which was developed at Bonn university for another experiment. This would also allow to take advantage of the time structure of the DORIS beam, which has only one bunch every 100 ns, so that the trigger system could operate synchronously with the bunch clock.

2.2.6 Performance

The experiment was simulated with a GEANT Monte-Carlo code, BLASTMC, which was written for the BLAST experiment and is known to be in very good agreement with BLAST elastic scattering data from hydrogen at 0.85 GeV incident energy. BLASTMC includes a full reconstruction of the charged particle tracks using the measured BLAST magnetic field. The vertex was generated with a triangular distribution function, following the target density distribution function.

The scattered electron momentum resolution (1σ), averaged over the complete acceptance) at 2 GeV incident energy is determined to be 70 MeV from BLASTMC simulations. Further, at larger scattering angles ($> 50°$) it drops to below 50 MeV. Thus, OLYMPUS will have the ability to clearly reject events where a pion is produced, in addition to an electron/positron and proton in the final state. The angular resolution is determined to be about $0.3°$ which will allow tight angular and coplanarity cuts on the final state electron/positron and proton.

Given the expected performance at 2 GeV with BLAST, it is probable that the BLAST toroidal field can be reduced from the maximum value, assumed above. A final decision on the field strength will be made when commissioning BLAST. Note that the resolutions are linear in the field but that the power cost is quadratic.

Figure 2.15 shows an elastic scattering event from hydrogen in BLAST at 0.85 GeV incident energy. Figure 2.16 shows the highly correlated elastic scattering elastic events when plotted as a function of final state scattering angles.

2.3 The internal gas target

The OLYMPUS internal hydrogen gas target will be of the type used in the HERMES and BLAST experiments. It will consist of a thin-walled (50 μm) aluminum storage cell with tubes of cylindrical cross section for the circulating DORIS beam, fed by an unpolarized gas feed system. The optics of the stored beam in DORIS determine the transverse dimensions of the cross section of the storage cell to be 9 mm vertically and 25 mm horizontally. The hydrogen gas diffuses slowly out of the cell and is pumped away by a large system of vacuum pumps at each end of the target. The cell wall will be cryogenically cooled to 25 K to increase the thickness of the target. The target will have a thickness of 3×10^{15} atoms/cm^2. The target will include Wakefield suppressors to minimize heating due to Wakefield.
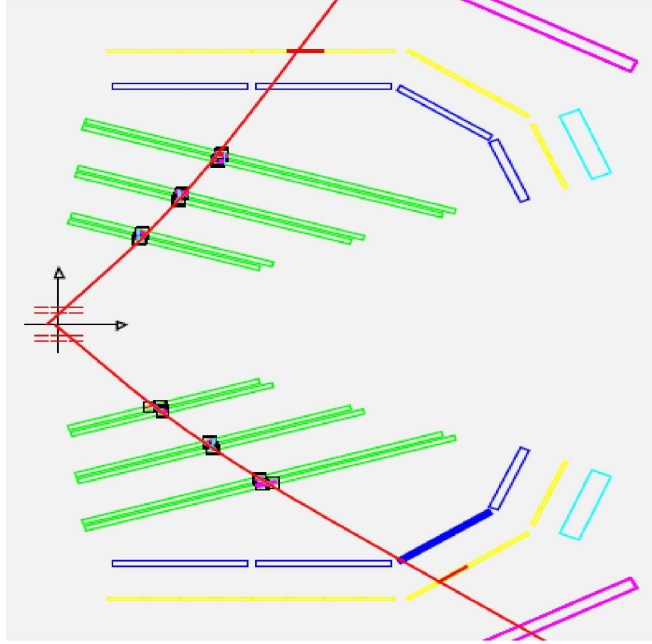
Figure 2.15: Sample electron-proton elastic scattering event.

A large three-stage turbo-molecular vacuum pumping system on each side of the target will be installed to reduce the vacuum pressure in the beamline. Vacuum pumps from BLAST, as shown in Figure 2.18, will be used.

The hydrogen gas will be fed to the storage cell using a system of valves and mass flow controllers. The feed system is shown schematically in figure 2.19.

A system of collimators will be required to minimize background in the detector. This will consist of a heavy metal fixed collimator directly in front of the target as well as movable beam scrapers in the DORIS ring. The transverse dimensions of the fixed collimator will be slightly smaller than those of the storage cell to minimize scattering into the detector. The beam scrapers will be adjusted after injection to minimize halo scattering near the experiment.

2.4 Monitoring the Luminosity

For the purpose of monitoring the luminosity with elastic scattering at small Q^2 and large ϵ, where the effects of two-photon exchange are negligible, it is proposed to utilize tracking telescopes at forward angles based on GEM technology.

The telescopes will be used to reconstruct the tracks of the lepton, in coincidence with the proton track reconstructed from the wire chamber information in the BLAST detector. For a clean event selection of elastic scattering, the polar and azimuthal angles of the lepton track will be correlated with those of the recoiling proton and with the proton's measured momentum. Additional elastic event selection redundancy is achieved by correlating the recorded times of the lepton and proton events. A prescaled fraction of single-arm events in the forward telescopes will also be recorded, which will be another independent rate
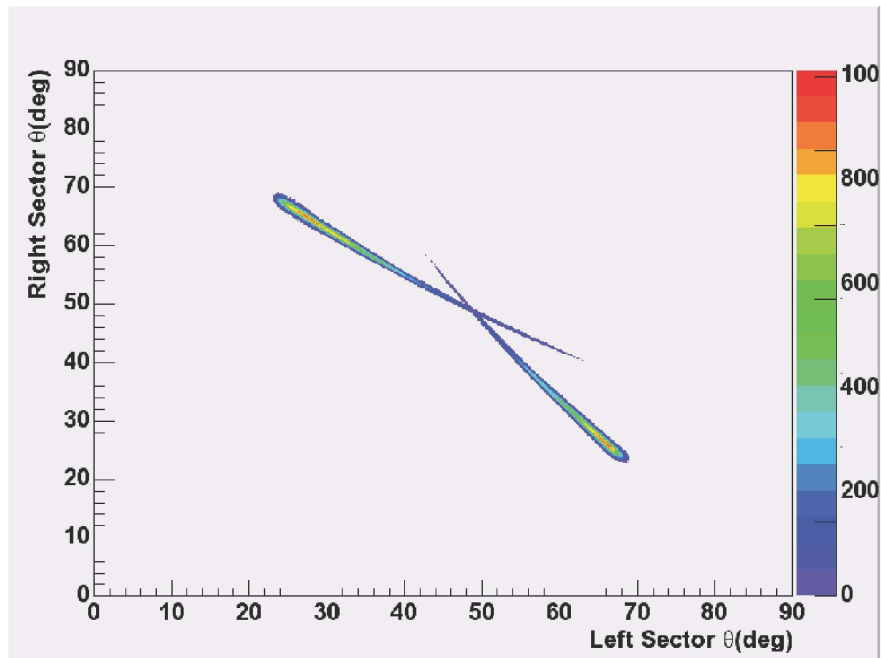
Figure 2.16: Elastic scattering electron-proton coincident events at 0.85 GeV incident energy.

measurement proportional to the luminosity.

Two telescopes will measure lepton tracks at a forward angle of $\approx 10°$, one in each of the two horizontal sectors, set up symmetrically. Each telescope will consist of three tracking planes, each tracking plane provided by a triple GEM detector. It will be required to fully reconstruct the lepton track, *i.e.* the polar and azimuthal angles θ and ϕ, and the vertex coordinate along the target z. The use of three tracking planes will allow to determine a track segment at forward angle, which is given by the position of the lepton track and its direction in three-dimensional space (i.e. the polar and azimuthal angles). The redundancy of a third tracking plane will increase accuracy and ease the alignment and calibration of the telescope. Although at forward angle the field integral is reduced compared to the standard BLAST setup, there will be a slight curvature of the tracks. The elastic scattering process allows to infer the lepton momentum from the proton track information, which will be used in the reconstruction of the lepton track parameters at the target back through the BLAST magnetic field.

The angular resolution of the lepton needs to be better than 0.5°; likewise, the resolution of the reconstructed vertex needs to be better than 1 cm in order to match the resolution for the proton track obtained from the wire chamber information. Using scintillator hodoscopes instead of GEM telescopes can not provide high enough angular and vertex resolution for this specific setup with an extended target and curved tracks.

Behind the position-sensitive element a fast plastic scintillator will be used to provide fast timing and trigger information. The three tracking planes will be at a distance of 160 cm from the target, centered at 10° facing the target for perpendicular impact angle, see Fig. 1.8. Each telescope will cover a solid angle of 3.9 msr, which will be achieved by choosing the active areas of the GEM planes to be 10×10 cm^2. Adopting the readout pattern of the
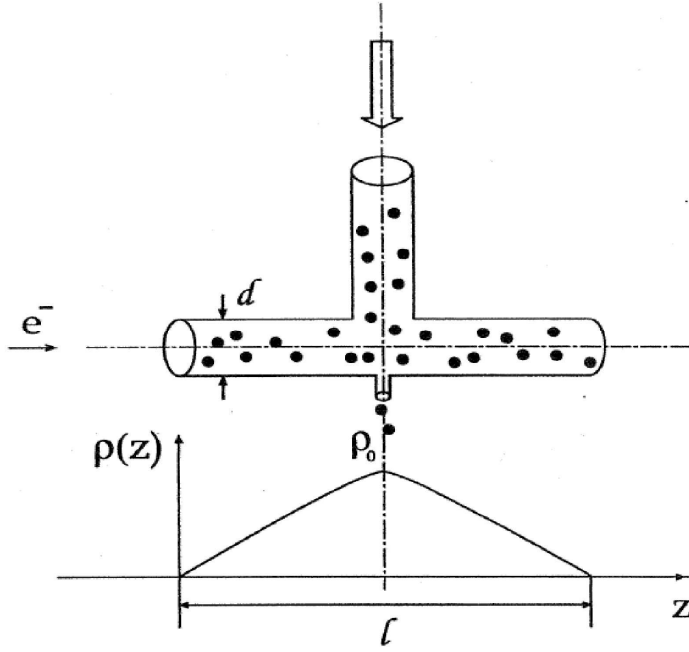
Figure 2.17: The principle of the internal gas target. The density profile along the target cell is approximately triangular.

MIT prototype [38] with strips along the x and y directions and a pitch of 635 μm, each plane will consist of $\approx 2 \times 160$ strips in x and y, a total of 3×320 channels per telescope. The MIT prototype telescope [38] has a proven resolution around 70 μm.

For the front-end electronics, the APV-25 chip will be used which can process up to 128 channels, however only 64 channels were used in the prototype (chosen to simplify manufacturing). The three tracking planes per telescope will require 2×3 APV chips per tracking plane or 18 APV chips per telescope. The APV chips are hosted on a hybrid board which, combined with the GEM control unit, is used to digitize the charge information and provide a buffered readout using FPGA technology.

Using the existing design for GEM detectors already developed at MIT including readout and control electronics greatly facilitates the production of the luminosity monitors. It also has the advantage that production costs are lower and implementation of a working design would be simpler.

The three triple-GEM detectors in each sector for the luminosity monitor and the possible GEM upgrade for the wire chambers can share a common gas system. For the BLAST wire chambers, a helium-isobutane gas mixture was chosen to minimize multiple scattering. However, at the energies proposed for operating OLYMPUS at DORIS this is not necessary and a non-flammable gas mixture like argon:carbon dioxide can be used.

The tracking telescopes will not require any collimation to define the solid angle; instead, all tracks will be reconstructed and the solid angle be defined by software cuts.
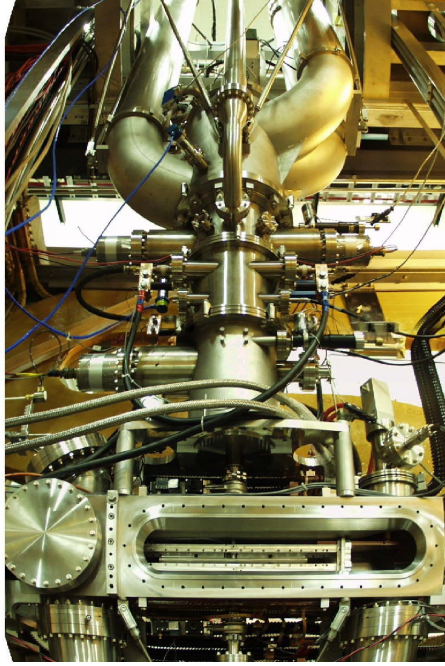
Figure 2.18: Photo of the BLAST target.

2.5 Backgrounds

The backgrounds in an internal gas target experiment at multi-GeV energies are well understood in experiments designed and successfully carried out by members of the collaboration. From both the BLAST (incident energy 0.85 GeV) and HERMES (incident energy 27 GeV) experiments, it is known that the backgrounds arise from the following sources:

1. showering of beam particles in beam pipe, the target cell and the vicinity of the experiment;

2. synchrotron radiation production in magnetic elements upstream of the experiment;

3. scattering from the atomic electrons in the target gas, *i.e.* Møller/Bhabha scattering;

4. electroproduction processes from the target.

for which we have the following solutions:

1. is suppressed by the presence of the fixed collimator directly in front of the target cell, the movable beam scrapers in the storage ring, and by careful tuning of the stored beam using scintillators and detectors near the internal target. Further, the toroidal magnetic field shields the detectors from electromagnetic shower products.

2. produces low energy photons which are prevented from striking the target cell by means of the fixed collimator.
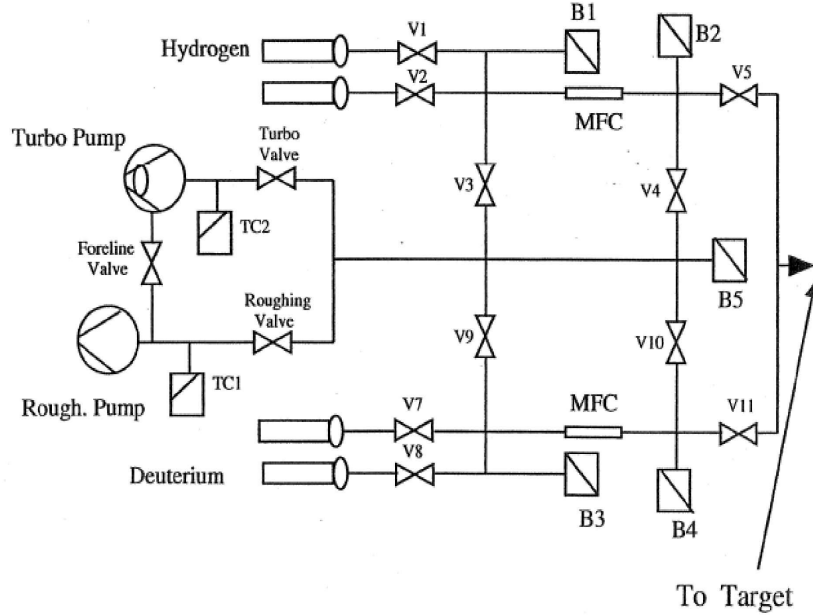
Figure 2.19: Schematic of the BLAST unpolarized gas feed system which can low both hydrogen and deuterium gas. MFC denotes a mass flow controller.

3. produces a high rate of scattered leptons. At large angles, the Møller/Bhabha leptons have low energies and do not make it out of the target. At forward angles their energies approach half of the incident beam energy but are peaked within $\theta \approx 1/\gamma$. The toroidal magnetic field and tracking chamber system of BLAST has been carefully designed so that Møller/Bhabha events are not a problem. The OLYMPUS trigger will demand a coincidence between scattered lepton and recoil proton in elastic scattering. The momenta and angles of both particles will be measured thus producing triple redundancy as the elastic process is completely determined by the measurement of any one of these quantities.

4. the primary background is the (e,e'π^0) process through the first resonance state of the proton. Estimates indicate that this background is $< 1\%$ of the elastic rate.

In summary, the proposed OLYMPUS experiment with optimally designed fixed shielding, movable collimators and carefully tuned, stored DORIS beam together with the toroidal BLAST spectrometer and detectors allowing clean coincidence detection of the scattered lepton and recoil proton, will not be affected by background.
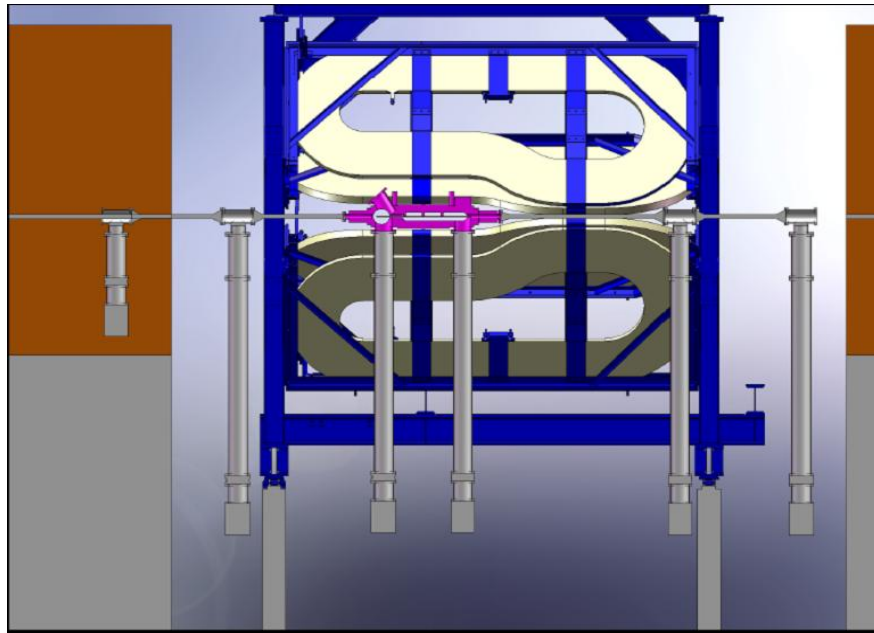
Figure 2.20: The internal gas target in the BLAST spectrometer at the present ARGUS interaction point.

Chapter 3

Logistics

3.1 Manpower

Arizona State University: R. Alarcon
DESY: F. Brinker, Y. Holler, and U. Schneekloth
Hampton University: M. Kohl
INFN, Bari: R. De Leo and E. Nappi
INFN, Ferrara: P. Ferretti Dalpiaz, P. Lenisa
INFN, Rome: D.M. Castelluccio, E. Cisbani, S. Frullani, F. Garibaldi, an L. Manfre
MIT: K. Dow, D. Hasell, J. Hays-Wehle, E. Ihloff, J. Kelsey, J. Matthews, R. Milner, R. Redwine, C. Tschalär, E. Tsentalovich, W. Turchinetz, J. van der Laan, and F. Wang
St. Petersburg Nuclear Physics Institute: S. Belostotski, G. Gavrilov, A. Izotov, A. Kisselev, P. Kravchenko, S. Manaenkov, O.Miklukho, Yu.Naryshkin, V.Vikhrov, D.Veretennikov
Universität Bonn: R. Beck, J. Hannappel, Ph. Hoffmeister, F. Klein, H. Schmieden, and N.N. (graduate students)
University of Colorado: E. Kinney
Universität Erlangen-Nürnberg: E. Steffens
University of Glasgow: R. Kaiser, G. Roser, and B. Seitz
University of Kentucky: C. Crawford
Universität Mainz: S. Baunack, A. Denig, D. von Harrach, F. Maas, M. Ostrick, N.N. (1 post-doc), and N.N. (Ph.D. students)
University of New Hampshire: J. Calarco

3.2 Institutional Responsibilities

Arizona State University: Particle identification
DESY: Installation
Hampton University: Luminosity monitor
INFN, Bari: GEM Electronics
INFN, Ferrara: Target
INFN, Rome: GEM electronics

EQUIPMENT	COST
	k$
target	450
BLAST toroid shipping	500
luminosity monitor	120
trigger electronics	80
wire chamber upgrade	75
on-line system	70

Table 3.1: Equipment with costs.

MIT: BLAST spectrometer, wire chambers, wire chamber upgrade, target, simulations
St. Petersburg Nuclear Physics Institute:
Universität Bonn: Trigger and data acquisition
University of Colorado: Wire chambers
Universität Erlangen-Nürnberg: Target
University of Glasgow: Particle identification
University of Kentucky: Simulations
Universität Mainz: Trigger, data acquisition, GEM detectors
University of New Hampshire: Timing scintillators

3.3   Budget

The equipment necessary to undertake the OLYMPUS experiment is costed in Table 3.1

The investment to modify the DORIS beamline, to implement fast switching from positrons to electrons, to install additional quadrupole magnets, for shielding, cabling, and cooling is estimated at 728 kEuro.

The power costs to operate DORIS are estimated at 150 kEuro/month at 2 GeV energy. The total cost of three months of dedicated data taking is estimated at 450,000 Euro.

The running costs for the OLYMPUS experiment are estimated at 160 kEuro/month assuming operation of BLAST at maximum field.

3.4   Timescale

The timescale is determined by the approval process at DESY and the availability of funding for the collaborating institutions. It is planned to submit funding requests by individual groups in Fall 2008. It is estimated that it will take one year after funding is approved before the OLYMPUS experiment can be installed at DESY. Assuming funding can be approved in Spring 2009, the experiment could begin data taking in summer 2010.

3.5   Requests to DESY

To carry out the proposed experiment we ask DESY to provide the following items:

1. Modification of the beamline in the vicinity of the ARGUS interaction region.

2. Construction and installation of a movable platform for the BLAST detector, including rails.

3. Power supply for the BLAST toroid.

4. Design, construction, and installation of a collimator system.

5. Shielding house for the experiment.

6. General services including electrical, cabling, alignment, and cooling water.

7. Beam-time to commission OLYMPUS in parallel with light source operation

8. Three months of dedicated DORIS operation at an incident energy of 2.0 GeV preferably in two six week blocks not less than six months apart.

Bibliography

[1] R. Hofstadter, Rev. Mod. Phys. **28**, 214 (1956).

[2] M. Goeckeler *et al.*, Phys. Rev. D **71**, 034508 (2005); C. Alexandrou, G. Koutsou, J.W. Negele, and A. Tsapalis, Phys. Rev. D **74**, 034508 (2006); J.D. Ashley *et al.*, Eur. J. Phys. **A19**(Suppl. 1), 9 (2004); H.H. Matevosyan *et al.*, Phys. Rev. C **71**, 055204 (2005).

[3] M.N. Rosenbluth, Phys. Rev. **79**, 615 (1950).

[4] R.C. Walker *et al.*, Phys. Rev. D **49**, 5671 (1994); L. Andivahis *et al.*, Phys. Rev. D **50**, 5491 (1994); F. Borkowski *et al.*, Nucl. Phys. **A222**, 269 (1974); Nucl. Phys. **B93**, 461 (1975); W. Bartel *et al.*, Nucl. Phys. **B58**, 429 (1973); C. Berger *et al.*, Phys. Lett. **B35**, 87 (1971); J. Litt *et al.*, Phys. Lett. **B31**, 40 (1970); W. Bartel *et al.*, Phys. Lett. **B25**, 236 (1967); T. Janssens *et al.*, Phys. Rev. **142**, 922 (1966).

[5] M.E. Christy *et al.*, Phys. Rev. C **70**, 015206 (2004).

[6] I.A. Qattan *et al.*, Phys. Rev. Lett. **94**, 142301 (2005).

[7] V. Punjabi *et al.*, Phys. Rev. C **71**, 055202 (2005); Erratum-ibid. Phys. Rev. C **71**, 069902(E) (2005); M. Jones *et al.*, Phys. Rev. Lett. **84**, 1398 (2000); O. Gayou *et al.*, Phys. Rev. Lett. **88**, 092301 (2002); G. MacLachlan *et al.*, Nucl. Phys. **A764** , 261 (2006).

[8] G. Ron *et al.*, Phys. Rev. Lett. **99**, 202002 (2007). B. Hu *et al.* Phys. Rev. C **73**, 064004 (2006); S. Strauch *et al.*, Phys. Rev. Lett. **91**, 052301 (2003);

[9] B. Milbrath *et al.*, Phys. Rev. Lett. **80** , 452 (1998); Erratum-ibid. Phys. Rev. Lett. **82**, 2221(E) (1999).

[10] S. Dieterich *et al.*, Phys. Lett. **B500**, 47 (2001).

[11] T. Pospischil *et al.*, Eur. Phys. J. **A12** , 125 (2001).

[12] O. Gayou *et al.*, Phys. Rev. C **64**, 038202 (2001).

[13] M.K. Jones, *et al.*, Phys. Rev. C **74**, 035201 (2006).

[14] C.B. Crawford *et al.*, Phys. Rev. Lett. **98**, 052301 (2007).

[15] J. Friedrich and Th. Walcher, Eur. Phys. J. A **17**, 607 (2003).

[16] J.J. Kelly, Phys. Rev. C **70**, 068202 (2004).

[17] R. Bijker and F. Iachello, Phys. Rev. C **69**, 068201 (2004).

[18] F. Iachello, A.D. Jackson, and A. Lande, Phys. Lett. **B43**, 191 (1973).

[19] J. Arrington, Phys. Rev. C **69**, 022201(R) (2004).

[20] J. Arrington, Phys. Rev. **C71**, 015202 (2005).

[21] J. Arrington *et al.*, *A measurement of two-photon exchange in unpolarized elastic electron-proton scattering*, Jefferson Lab Proposal E05-017 (2005).

[22] C. Perdrisat *et al.*, Jefferson Lab Proposals E01-109, E04-108.

[23] J. Arrington *et al.*, Conceptual Design Report CD0, Hall C 12 GeV Upgrade (2002).

[24] P.A.M. Guichon and M. Vanderhaeghen, Phys. Rev. Lett. **91**, 142303 (2003); P.G. Blunden, W. Melnitchouk, and J.A. Tjon, Phys. Rev. Lett. **91**, 142304 (2003); M.P. Rekalo and E. Tomasi-Gustafsson, Eur. Phys. J. **A22**, 331 (2004); Y.C. Chen, A.V. Afanasev, S.J. Brodsky, C.E. Carlson and M. Vanderhaeghen, Phys. Rev. Lett. **93**, 122301 (2004); A.V. Afanasev and N.P. Merenkov, Phys. Rev. D **70**, 073002 (2004); A.V. Afanasev *et al.*, Phys. Rev. D **72**, 013008 (2005).

[25] P.G. Blunden, W. Melnitchouk, and J.A. Tjon, Phys. Rev. C **72**, 034612 (2005).

[26] S. Kondratyuk, P. Blunden, W. Melnitchouk, and T.A. Tjon, Phys. Rev. Lett. **95**, 172503 (2005).

[27] Yu.M. Bystritskiy, E.A. Kuraev, and E. Tomasi-Gustafsson, Phys. Rev. C **75**, 015207 (2007).

[28] P. Bosted, Phys. Rev. **C51**, 409 (1995).

[29] J. Mar *et al.*, Phys. Rev. Lett. **21**, 482 (1968).

[30] J. Arrington *et al.*, *Beyond the Born Approximation: A Precise Comparison of e^+p and e^-p Elastic Scattering in CLAS*, PR04-116, PAC26 (2004)

[31] J. Arrington *et al.*, *Two photon exchange of electrons/positrons on the proton*, Proposal at VEPP-3, nucl-ex/0408020 (2004).

[32] S. Kowalski *et al.*, *Measurement of the Two-Photon Exchange Contribution in ep Elastic Scattering Using Recoil Polarization*, Jefferson Lab Proposal E04-019 (2004).

[33] D.J. Margaziotis *et al.*, *Measurement of the Target Single-Spin Asymmetry in Quasi-Elastic $^3He^\uparrow(e,e')$*, Jefferson Lab Proposal E05-15, PAC27 (2005).

[34] D. Cheever *et al.*, Nucl. Instr. Meth. **A556** , 410 (2006).

[35] F. Weissbach *et al.*, Eur. Phys. J. **A30**, 477 (2006).

[36] C. Tschalaer, private communication.

[37] C. Altunbas *et al.*, Nucl. Instr. Meth. **A490**, 177 (2002).

[38] F. Simon *et al.*, arXiv:0808.3477v1, submitted to Nucl. Instr. Meth.

[39] G. Höhler *et al.*, Nucl. Phys. **B114**, 505 (1976).

[40] K. Dow *et al.*, to be published.

[41] F. Sauli, "GEM: A new concept for electron amplification in gas detectors", Nucl. Instr. and Meth. **A386**, 531 (1997).

[42] M.C. Altunbas *et al.*, "Construction, test and commissioning of the triple-GEM tracking detector for COMPASS", Nucl. Instr. and Meth. **A490**, 177 (2002).